



# Generation of ultrashort UV pulses and R2PI measurements of deflected molecules

(Erzeugung von ultrakurzen UV Pulsen und R2PI Messungen von räumlich abgelenkten Molekülen)

vorgelegt von  
Lena Worbs  
geboren am  
21. April 1993  
in Bad Oldesloe

Bachelorarbeit im Studiengang Physik  
Universität Hamburg  
Center for Free-Electron Laser Science (CFEL)

2015

1. Gutachter: Prof. Dr. Jochen Küpper
2. Gutachter: Dr. Daniel Horke



hallo

Hiermit bestätige ich, dass die vorliegende Arbeit von mir selbstständig verfasst wurde und ich keine anderen als die angegebenen Hilfsmittel – insbesondere keine im Quellenverzeichnis nicht benannten Internetquellen – verwendet habe und die Arbeit von mir nicht vorher in einem anderen Prüfungsverfahren eingereicht wurde. Die eingereichte schriftliche Form entspricht der auf dem elektronischem Speichermedium. Ich bin damit einverstanden, dass die Bachelorarbeit veröffentlicht wird.

Hamburg, den 14. September 2015



*"Zwei mal drei macht vier."*  
- Pippi Langstrumpf



## Abstract

This thesis is about the generation and characterization of ultrashort ultraviolet (UV) laser pulses, resonance-enhanced two photon ionization (R2PI) measurements of indole and the electrostatic deflection of indole.

UV pulses are generated from a 39 fs Ti:Sapphire Laser with a central wavelength of 800 nm and a bandwidth of 60 nm. To generate UV pulses, the nonlinear process of harmonic generation in a beta-barium-borate (BBO)-crystal is used. A prism compressor ensures group velocity dispersion (GVD) compensation and a cross correlation is used to measure the pulse duration of the generated UV pulses. An energy conversion efficiency of up to 6 % of the fundamental energy is achieved to produce UV pulses and the generated pulses have a theoretical minimum pulse duration of 35 fs due to the spectrum.

R2PI measurements are used to identify the fragmentation of indole ( $\text{C}_8\text{H}_7\text{N}$ ) at UV pulses in comparison to the fragmentation at IR pulses. Additionally, the spatial deflection of indole due to an electric field is measured.

The time of flight mass spectra (TOF MS) of indole show great differences when the molecule is ionized by IR or UV pulses, respectively. With UV pulses it is possible to ionize the molecule almost without fragments or background.





## **Zusammenfassung**

In der vorliegenden Arbeit werden ultrakurze UV Pulse erzeugt, resonanzverstärkte Mehrphotonenionisations-Messungen (REMPI measurements) an Indol durchgeführt und die räumliche Ablenkung von Indol in einem elektrischen Feld betrachtet. UV Pulse werden durch nichtlineare optische Effekte (Frequenzverdopplung) in Beta Barium Borat (BBO) erzeugt. Ausgangspunkt ist ein Ti:Saphir Laser mit einer Pulsdauer von 39 fs. Um die auftretende Gruppengeschwindigkeitsverzögerung (GVD) zu kompensieren, wird ein Prismen Kompressor verwendet. Mit Hilfe einer Kreuz Korrelation wird die Pulslänge der UV Pulse bestimmt.

Es wird eine Energieeffizienz von 6 % der Energie der Fundamentalen zur Erzeugung von UV Pulsen erreicht und eine theoretische minimale Pulsdauer von 35 fs auf Grund des Spektrums bestimmt.

Mit den erzeugten UV Pulsen werden R2PI Messungen durchgeführt, um den Zerfall von Indol ( $C_8H_7N$ ) durch UV Pulse im Vergleich zum Zerfall durch IR Pulse zu untersuchen. Ebenfalls wird die räumliche Ablenkung von Indol in einem elektrischen Feld gemessen.

Die Massenspektren von Indol bei einer Ionisation mit IR oder UV Pulsen weisen deutliche Unterschiede auf. Mit UV Pulsen ist eine Ionisation des Moleküls möglich, ohne Fragmente zu erzeugen oder den Hintergrund zu ionisieren.



# Contents

|          |   |           |
|----------|---|-----------|
| <b>1</b> | <b>Introduction</b>   | <b>1</b>  |
| <b>2</b> | <b>Theoretical Backgrounds</b>                                | <b>3</b>  |
| 2.1      | Linear Optics . . . . .                                       | 3         |
| 2.1.1    | Light Pulses . . . . .  | 4         |
| 2.1.2    | Relation between Duration and Spectral Width . . . . .        | 4         |
| 2.1.3    | Pulse Propagation of a Light Pulse in a Transparent Medium .  | 5         |
| 2.1.4    | Dispersion Parameter of a Transparent Medium . . . . .        | 6         |
| 2.1.5    | Time Compression . . . . .                                    | 7         |
| 2.2      | Nonlinear Optics . . . . .                                    | 9         |
| 2.2.1    | Second Harmonic Generation . . . . .                          | 9         |
| 2.2.2    | Sum Frequency Generation . . . . .                            | 11        |
| 2.2.3    | Self- Phase Modulation . . . . .                              | 11        |
| 2.3      | Ultrashort Laser Pulses . . . . .                             | 12        |
| 2.3.1    | Ti:Sapphire Laser . . . . .                                   | 12        |
| 2.3.2    | Pulse Duration Measurements . . . . .                         | 13        |
| 2.4      | Molecular Physics Basics . . . . .                            | 16        |
| 2.4.1    | Quantum States of Molecules . . . . .                         | 16        |
| 2.4.2    | REMPI Measurements of Molecules . . . . .                     | 17        |
| 2.4.3    | Mass Spectroscopy . . . . .                                   | 17        |
| 2.4.4    | Molecules in External Electric Fields . . . . .               | 18        |
| 2.4.5    | Indole . . . . .  | 19        |
| <b>3</b> | <b>Experimental Setup</b>                                     | <b>23</b> |
| 3.1      | Mobile Setup to Generate and Characterize UV Pulses . . . . . | 23        |
| 3.1.1    | Second and Third Harmonic Generation . . . . .                | 25        |
| 3.1.2    | Prism Compressor . . . . .                                    | 25        |
| 3.1.3    | Cross Correlation . . . . .                                   | 26        |
| 3.2      | Molecular Beam Machine for TOF Mass Spectroscopy . . . . .    | 26        |
| <b>4</b> | <b>Results and Discussion</b>                                 | <b>29</b> |
| 4.1      | Second and Third Harmonic Generation . . . . .                | 29        |

|          |  |           |
|----------|--|-----------|
| 4.2      | Auto and Cross Correlation . . . . .                     | 33        |
| 4.3      | Fragmentation of Indole . . . . .                        | 34        |
| 4.3.1    | Fragmentation at 800 nm pulses . . . . .                 | 34        |
| 4.3.2    | Fragmentation at 269 nm pulses . . . . .                 | 37        |
| 4.4      | Deflection of Indole . . . . .                           | 39        |
| <b>5</b> | <b>Conclusion</b>  | <b>41</b> |
| <b>A</b> | <b>Appendix</b>  | <b>49</b> |
| A.1      | Second Harmonic Generation . . . . .                     | 49        |
| A.2      | Fragmentation of Indole . . . . .                        | 50        |
| A.3      | Indole <sup>+</sup> Signal at TOF Measurements . . . . . | 51        |
| A.4      | Spatial Profiles Fit . . . . .                           | 51        |

# Chapter 1

## Introduction

Molecular physics is the basis of chemistry and biology. To understand and be able to manipulate chemical and biological processes, the structure and the dynamics of the participating molecules are essential.

Molecular spectroscopy is an important instrument to get information about the structure and dynamics of molecules. Additionally to the electronic energy states as known from atoms, molecules have vibrational and rotational energy states. The electronic transition energy of molecules is in the violet or ultraviolet region of the spectrum of light. The use of UV laser pulses is therefore desirable to get information about the electronic bond structure of a molecule. It is not effective to build UV lasers, because the Einstein coefficient  $B_{12}$  is related to the probability of stimulated absorption and is proportional to  $\lambda^3$ . For smaller wavelengths  $\lambda$ , it is not efficient to produce a population inversion, and for wavelengths in the UV region, it is even impossible [1]. For generating UV laser pulses, nonlinear optical processes can be used instead. A very important nonlinear effect is second harmonic generation (SHG). Using this effect, it is possible to double the frequency of a laser beam by the use of nonlinear crystals (e.g. BBO). With this effect, wavelengths in the UV range can be generated and can be used for molecular spectra measurements.

Electronic transitions and bond breaking happen on a femtosecond time scale, so a high time resolution is necessary. This can be achieved by the use of femtosecond pulse durations. A well-known commercial femtosecond laser is the Ti:Sapphire laser, which is emitting in the infrared with pulse durations of ten to hundred femtoseconds [2]. UV laser pulses can be generated from a Ti:Sapphire laser using third harmonic generation.

Indole ( $C_8H_7N$ ) is a part of the amino acid tryptophan. The emission properties of tryptophan are used in fluorescence experiments on proteins. Indole is one of the most important biological chromophores and responsible for the ability of tryptophan to absorb light around 300 nm [3]. Therefore, indole is of great interest [4].

The ionization energy of indole is 7.76 eV [5]. This energy is equal to photons with a wavelength of about 160 nm. The third harmonic of a Ti:Sapphire laser has a wavelength of 266 nm, meaning two photons are necessary to ionize this molecule.

# Chapter 2

## Theoretical Backgrounds

This chapter is about the theoretical background of the physical effects which are necessary to understand third harmonic generation, pulse compression and pulse duration measurements as well as the time of flight (TOF) resonance-enhanced multiphoton ionization (REMPI) measurements of indole.

The chapters [2.1 - 2.3.2] are written according to [6] and [7] and the molecular physics chapter [2.4] is written according to [8].

### 2.1 Linear Optics

An electromagnetic wave is described by the Maxwell-equations. When the magnetic field amplitude is much less than the electric field amplitude, the propagation of light can be described by the following second order differential equation:

$$\nabla^2 \mathbf{E} = \frac{1}{c^2} \frac{\partial^2 \mathbf{E}}{\partial t^2}, \text{ with } \frac{1}{c^2} = \mu_r \epsilon_0, \quad (2.1)$$

where  $\mathbf{E}$  is the electric field,  $c$  the velocity of light,  $\mu_r$  the permeability and  $\epsilon_0$  the permittivity.

The solutions for this differential equation are plane waves. Without loss of generality, the propagation of a transverse electric field  $E_y$  along the  $x$ -axis is determined by

$$E_y = \text{Re} \left( E_0 \cdot e^{i\omega(t - \frac{x}{c})} \right) = \text{Re} \left( E_0 \cdot e^{i(\omega t - \mathbf{k} \cdot \mathbf{r})} \right). \quad (2.2)$$

$E_0$  is the electric field amplitude,  $\omega$  the angular frequency,  $t$  the time,  $\mathbf{k}$  the wave vector and  $\mathbf{r}$  the distance from the origin. The amplitude varies with a cosine in time with an angular frequency  $\omega$ .

Waves as a pure sine or cosine are infinite, so their spectrum contains only one frequency and can mathematically be described as a  $\delta$ -distribution. A plane wave is the absolute opposite of a light pulse, so a light pulse does not consist of a single

frequency and can not be described as a  $\delta$ -distribution.

### 2.1.1 Light Pulses

To describe a light pulse, assuming its envelope is Gaussian,  $E_y$  is simply multiplied with a Gaussian function. The resulting equation is:

$$E_y = \text{Re} \left( E_0 e^{-\Gamma t^2 + i\omega t} \right), \quad (2.3)$$

where  $\Gamma$  is the shape factor of the Gaussian envelope. Fig. [2.1] shows a Gaussian light pulse in the time domain.

The Fourier transform of  $E_y$  contains the spectral nature of the light pulse. The Fourier transform of a Gaussian pulse is still a Gaussian function.

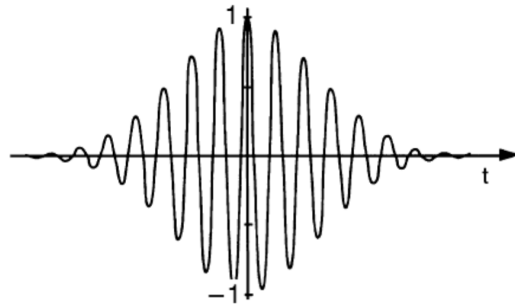


**Fig. 2.1:** Time evolution of the electric field in a Gaussian pulse. Adapted from [6].

### 2.1.2 Relation between Duration and Spectral Width

The general time and frequency Fourier transforms of a pulse, without assuming any pulse shape, are given by

$$\epsilon(t) = \frac{1}{2\pi} \int_{-\infty}^{\infty} E(\omega) e^{-i\omega t} d\omega \quad (2.4)$$

$$E(\omega) = \int_{-\infty}^{\infty} \epsilon(t) e^{-i\omega t} dt. \quad (2.5)$$

It can be shown [7], that duration and spectral width are related through the inequality:

$$\Delta t \Delta \omega \geq \frac{1}{2}. \quad (2.6)$$

This result is all classical, but shows quantum mechanics as well. The pulse duration cannot be exactly determined by measuring the spectral bandwidth of a pulse.

In experiments, it is easier and more accurate to use half-maximum quantities:

$$\Delta \nu \Delta t = K, \quad (2.7)$$



with  $\Delta\nu$  as full width at half maximum (FWHM) and  $K$  as a factor which depends on the assumed pulse shape.

### 2.1.3 Pulse Propagation of a Light Pulse in a Transparent Medium

As shown above (see ch. [2.1.2]), ultrashort laser pulses must have a large spectral bandwidth. Due to group velocity dispersion (GVD) in media, phase distortion with an increase of the pulse duration will happen.

The frequency Fourier transform of a Gaussian pulse is

$$E_0(\omega) = \exp\left(\frac{-(\omega - \omega_0)^2}{4\Gamma}\right). \quad (2.8)$$

After propagating the distance  $x$  in a medium, the spectrum is modified to

$$E(\omega, x) = E_0(\omega) \exp(-ik(\omega)x), \quad (2.9)$$

with  $k(\omega) = \frac{n\omega}{c}$  as the frequency dependent propagation factor.

Rewriting  $k(\omega)$  as a Taylor expansion, assuming that  $\Delta\omega \ll \omega_0$ , gives

$$k(\omega) = k(\omega_0) + k'(\omega - \omega_0) + \frac{1}{2}k''(\omega - \omega_0)^2 + \dots, \quad (2.10)$$

with  $k' = \left(\frac{dk(\omega)}{d\omega}\right)_{\omega_0}$  and  $k'' = \left(\frac{d^2k(\omega)}{d\omega^2}\right)_{\omega_0}$ .

The resulting electric field can be written as

$$E(\omega, x) = \exp\left(-ik(\omega_0)x - ik'x \cdot (\omega - \omega_0) - \left(\frac{1}{4\Gamma} + \frac{i}{2}k''\right)(\omega - \omega_0)^2\right). \quad (2.11)$$

The time evolution is given by the Fourier transform

$$\epsilon(t, x) = \sqrt{\frac{\Gamma(x)}{\pi}} \cdot \exp\left(i\omega_0\left(t - \frac{x}{v_\phi(\omega_0)}\right)\right) \cdot \exp\left(-\Gamma(x)\left(t - \frac{x}{v_g(\omega_0)}\right)^2\right), \quad (2.12)$$

with  $v_\phi(\omega_0) = \left(\frac{\omega}{k}\right)_{\omega_0}$  as the phase velocity,  $v_g(\omega_0) = \left(\frac{d\omega}{dk}\right)_{\omega_0}$  as the group velocity and  $\frac{1}{\Gamma(x)} = \frac{1}{\Gamma} + 2ik''x$ .

Looking at the first exponential term in eq. [2.12], the phase of the central frequency  $\omega_0$  is delayed by  $\frac{x}{v_\phi}$  after propagating the distance  $x$ . The phase is not a measurable quantity, thus it does not have observable consequences.

The second exponential term describes still a Gaussian pulse shape after propagating the distance  $x$ . The Gaussian envelope is delayed by  $\frac{x}{v_g}$ .

In ordinary matter, the group velocity is smaller than the phase velocity:  $v_g < v_\phi$ . With  $k = \frac{2\pi}{\lambda}$  and the wavelength in a medium  $\lambda = \frac{2\pi c}{\omega}n(\omega)$ , where  $n(\omega)$  is the index

of refraction, one can find the following equation:  $v_\phi = \frac{c}{n(\omega)}$ .

With  $v_g = \frac{d\omega}{dk}$ , the group and phase velocity are related to each other by

$$v_g \approx v_\phi \left( 1 - \frac{\omega}{n(\omega)} \frac{dn(\omega)}{d\omega} \right). \quad (2.13)$$

Because of the form factor  $\Gamma(x)$ , the pulse envelope is distorted during the propagation in the medium due to its dependence of  $\omega$  through  $k''$ .  $k''$  is called group velocity dispersion (GVD).

To see how the shape of the pulse changes,  $\Gamma(x)$  can be rewritten as

$$\Gamma(x) = \frac{\Gamma}{1 + \xi^2 x^2} - i \frac{\Gamma \xi x}{1 + \xi^2 x^2}, \quad (2.14)$$

where  $\xi = 2\Gamma k''$ .

Substituting this into the second exponential term in eq. [2.12], the term yields to the following expression

$$\exp \left( -\frac{\Gamma}{1 + \xi^2 x^2} \left( t - \frac{x}{v_g} \right)^2 + i \frac{\Gamma \xi x}{1 + \xi^2 x^2} \left( t - \frac{x}{v_g} \right)^2 \right). \quad (2.15)$$

This equation still describes a delayed Gaussian function. The form factor is now  $\frac{\Gamma}{1 + \xi^2 x^2}$  which is always smaller than  $\Gamma$ , so the pulse undergoes a duration broadening. Taking the imaginary part into consideration, the phase contains a quadratic term of time, which is a linear frequency chirp.

To sum up: The propagation of a short pulse in transparent medium results in a delay of the pulse, a duration broadening and a frequency chirp.

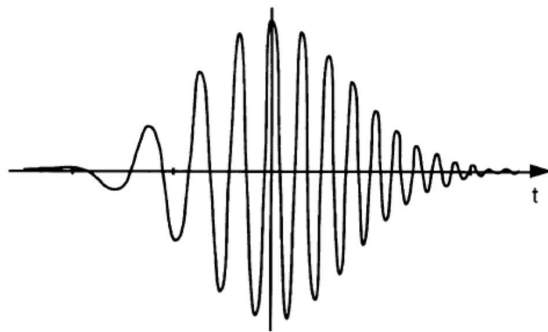


**Fig. 2.2:** Time evolution of the electric field in a chirped Gaussian pulse. The leading part is red shifted and the trailing part blue shifted. Adapted from [6].

### 2.1.4 Dispersion Parameter of a Transparent Medium

The dispersion can be recalculated as a function of wavelength, due to the often used wavelength dependence of material quantities (e.g. the refractive index).

Taking the GVD  $k'' = (\frac{d^2 k(\omega)}{d\omega^2})_{\omega_0}$ , one obtains

$$k'' = -\frac{\lambda^2}{2\pi c} D, \quad (2.16)$$

where  $D = \frac{1}{L} \frac{dt_g}{d\lambda}$  is the dispersion parameter and  $t_g$  is the group delay induced by propagation over length  $L$ , so that  $t_g = \frac{L}{v_g}$ . With these quantities,  $k''$  is

$$k'' = \frac{\lambda^3}{2\pi c^2} \frac{d^2 n}{d\lambda^2} \quad (2.17)$$

Usually (e.g. in glass or in air), the wavelength is larger than the resonance wavelength, which means the GVD is positive ( $k'' > 0$ ). With increasing wavelength, the index of refraction diminishes, so the group velocity increases.

When the wavelength is below the electronic resonance, the situation is reversed and the GVD is negative.

### 2.1.5 Time Compression

The spectrum of a short pulse consists of different wavelengths due to the relation between pulse duration and spectral width (see ch. [2.1.2]), which leads to group velocity dispersion distortion while traveling through transparent media (see ch. [2.1.3]). Optical devices with an overall negative GVD: e.g. a pair of transmission gratings or four prisms can reverse the effect.

The following section is about the time compression by a prism compressor. For compression with gratings see [2].

Angular dispersion leads to negative GVD, so prisms can be used for time compression. A setup for a prism compressor consisting of four prisms is shown in fig. [2.3].

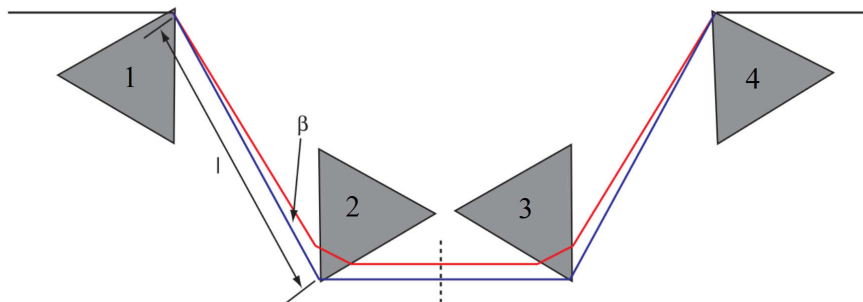


**Fig. 2.3:** Schematic overview of a prism compressor built of four prisms. The dashed line between prisms 2 and 3 shows an optional mirror, so only two prisms are needed to achieve the same time compression effect. Adapted from [9], slightly modified by numbering the prisms.

The incoming pulses enter and leave all prisms at Brewster angle. This angle ensures minimum reflection losses for p polarization at the surfaces. The first prism

disperses the beam. The second one collimates it and prisms 3 and 4 undo the dispersion of 1 and 2. Because of the different pathways of blue and red shifted frequencies, the pulse duration decreases. At the dashed line, a mirror can be placed, so that the prism compressor only consists of two instead of four. A two prism prism compressor is easier to align.

The incoming beam will be split up in its wavelengths, so that the traveling path is wavelength dependent:

$$P = 2l \cdot \cos(\beta), \quad (2.18)$$

where  $l$  is the distance between apex 1 and 2 and  $\beta$  is the angle of the dispersed beam (see fig. [2.3]).

The group delay dispersion (GDD) introduced by this prism sequence is

$$\text{GDD}_{\text{prism}} = \left( \frac{\lambda^3}{2\pi c^2} \right) \frac{d^2 P(\lambda)}{d\lambda^2}. \quad (2.19)$$

With approximations for the angle  $\beta$  and therefore for the traveling path  $P$  [9], eq. [2.19] simplifies to

$$\text{GDD}_{\text{prism}} = \frac{\lambda^3}{2\pi c^2} \left( -4l \left( 2 \left( \frac{dn}{d\lambda} \right)^2 \right) + 4 \left( \frac{d^2 n}{d\lambda^2} \right) (2D_{1/e^2}) \right), \quad (2.20)$$

where  $D_{1/e^2}$  is the diameter of the beam.

The GDD is also determined by the product of the length of the material and the GVD.

$$\text{GVD} = \frac{\lambda^3}{2\pi c^2} \left( \frac{d^2 n}{d\lambda^2} \right). \quad (2.21)$$

When it is obvious which optics are responsible for GDD, it can be calculated and the equation for the distance of prisms can be solved. Otherwise, the pulse duration can be measured before and after the optics and the distance can be calculated.

## 2.2 Nonlinear Optics

The difference between linear and nonlinear optics is the intensity dependence of optical quantities. When light passes through a medium, an external electric field enters the medium. The electrons are excited and accelerate around their zero position. Taking one atom into account, a microscopic dipole moment  $\boldsymbol{\rho}$  appears

$$\boldsymbol{\rho} = -\alpha \mathbf{E}, \quad (2.22)$$

where  $\alpha$  is the polarizability of the atoms. To get the macroscopic dipole moment, all microscopic moments have to be summed up:

$$\mathbf{P} = \sum_i \frac{\boldsymbol{\rho}_i}{V}. \quad (2.23)$$

The oscillation of the electric field results in an oscillation of the electrons. The response of the electrons on the external electric field is the polarization. For small electric field intensities the oscillation is approximatively harmonic, so the relation between the electric field and the oscillating polarization is:

$$\mathbf{P}(\omega) = \epsilon_0 \chi(\omega) \mathbf{E}(\omega), \quad (2.24)$$

where  $\chi$  as the susceptibility describes the properties of the material in an external field dependent on the frequency and determines the polarization.

When having electric fields with high intensities, the electrons are moving more, so they get into the anharmonic region of their potential, which leads into anharmonic movements instead of linear polarization. To consider this, a polynomial expansion of the macroscopic polarization  $P = |\mathbf{P}|$  of a medium can be done:

$$\frac{P}{\epsilon_0} = \underbrace{\chi^{(1)} \cdot E}_{\text{index, absorption}} + \underbrace{\chi^{(2)} \cdot E \cdot E}_{\text{SHG, parametric effects}} + \underbrace{\chi^{(3)} \cdot E \cdot E \cdot E}_{\text{THG, SPM, nonlinear index}} + \dots, \quad (2.25)$$

where SHG means second harmonic generation (ch. [2.2.1]), THG stands for third harmonic generation and SPM is self phase modulation (ch. [2.2.3]).

### 2.2.1 Second Harmonic Generation

Second harmonic generation (SHG) is one of the most important nonlinear optical effects. An incoming fundamental wave with a frequency  $\omega_1$  (wavelength  $\lambda_1$ ) can generate a second harmonic wave with twice the frequency (half the wavelength) in a nonlinear crystal. Therefore, two photons with frequency  $\omega_1$  are mixed in a nonlinear crystal (e.g. a BBO-crystal) and generate a third photon with frequency

$\omega_2 = 2 \cdot \omega_1$  (see fig. [2.4]). For mathematical description see [A.1].

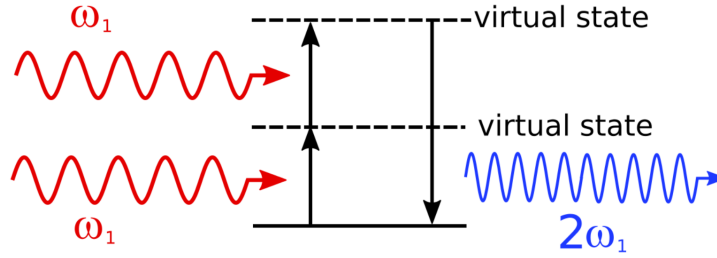


**Fig. 2.4:** The process of second harmonic generation in energy levels. Two photons are exciting an electron to virtual states. While going back to the initial state, a photon with twice the frequency is emitted.

When photons enter an optical medium, an external electric field appears to the electrons in the medium. The electrons are stimulated and perform harmonic electronic dipole oscillations. When the electric field is strong enough, the oscillations become anharmonic.

In the ideal case of plane waves, the intensity of the generated second harmonic is

$$I(2\omega) = \frac{2^7 \pi^3 \omega^2 \chi_{\text{eff}}^2 l^2}{n^3 c^3} I^2(\omega) \left( \frac{\sin(\Delta k l / 2)}{\Delta k l / 2} \right)^2. \quad (2.26)$$

$\chi_{\text{eff}}$  is the effective susceptibility and depends on the material,  $l$  is the length of the material,  $n$  the index of refraction and  $\Delta k$  is the dephasing quantity. For SHG, materials with a large  $\chi_{\text{eff}}^2$  are used. To get maximum intensity, the dephasing quantity  $\Delta k$  has to be zero. If  $\Delta k$  is zero the two contributors add constructively, otherwise they would interfere destructively.

The condition  $\Delta k = 0$  is called phase-matching. In fig. [2.5] phase-matching is illustrated.

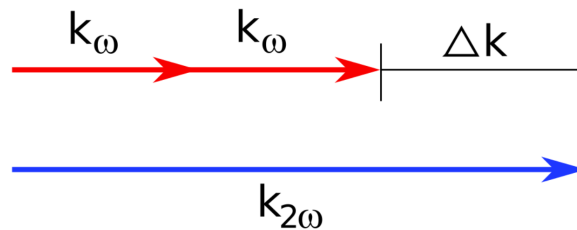


**Fig. 2.5:** Schematic illustration of phase matching. The wave vectors of the second harmonic with the wave vector  $k_{2\omega}$  and the sum of the fundamental wave vectors  $k_\omega$  must be equal to ensure constructive interference.

There are three types of crystals which can be used to generate harmonics:

- type 0/I : The mixing photons have same polarization, the resulting photon has a polarization orthogonal to the incoming polarization. At type 0, the

incoming photons have extraordinary polarization with respect to the optical axis of the crystal and the resulting photon has ordinary polarization. Type I is reversed.

- type II: The mixing photons have orthogonally polarizations. The resulting photons polarization is extraordinary.

SHG with ultrashort light pulses is based on the same principle, except from the doubling bandwidth of the crystal, which has to match the full spectrum of the incoming pulse.

### 2.2.2 Sum Frequency Generation

The process of SHG can happen with photons, which do not have the same frequency. This process is called sum frequency generation (SFG).

Two photons excite an electron to a virtual state. The emitting photon then has the frequency  $\omega_1 + \omega_2$  (see fig. [2.6]).

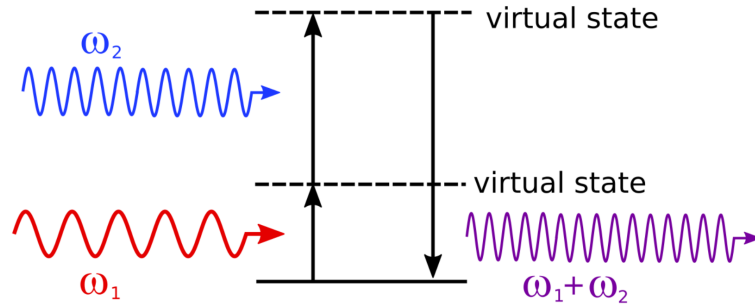


**Fig. 2.6:** The process of sum frequency generation in energy levels. Two photons with different frequencies  $\omega_1$  and  $\omega_2$  are exciting an electron to virtual states. While going back to the initial state, a photon is emitted, which has the frequency  $\omega_1 + \omega_2$ .

### 2.2.3 Self- Phase Modulation

When the electric field is strong enough, not only second order susceptibility effects occur, but also third or fourth order effects.

Self phase modulation (SPM) is a third order susceptibility effect. The nonlinear index of refraction of a material is dependent on the light pulses time dependent envelope. It can be expressed by

$$n = n_0 + \frac{1}{2}n_2I(t), \text{ with } I(t) = e^{-\Gamma t^2}. \quad (2.27)$$

If  $n_2$  is positive, new low frequencies are added in the leading part of the envelope and high frequencies in the trailing part. When the pulse travels through other transparent media, the group velocity dispersion will increase (see ch. [2.1.3]). SPM

is often an effect which is wanted to be prevented.

This effect can also be used for pulse compression to less than 10 fs in the visible spectral range.

## 2.3 Ultrashort Laser Pulses

The most common femtosecond laser is a Ti:Sapphire laser. The following sections will be about the generation of ultrashort pulses in a Ti:Sapphire laser and the characterization of ultrashort laser pulses. To characterize an ultrashort laser pulse this thesis determines its energy, its spectrum and its pulse duration.

### 2.3.1 Ti:Sapphire Laser

The gain medium of a Ti:Sapphire laser is titanium doped aluminum oxide ( $\text{Ti:Al}_2\text{O}_3$ ).  $\text{Ti}^{3+}$  ions are substitutes for  $\text{Al}^{3+}$  ions in the sapphire structure. The lasing action is due to the  $\text{Ti}^{3+}$ -ion. Its ground state is split into a pair of vibrationally broadened levels (see fig. [2.7]).

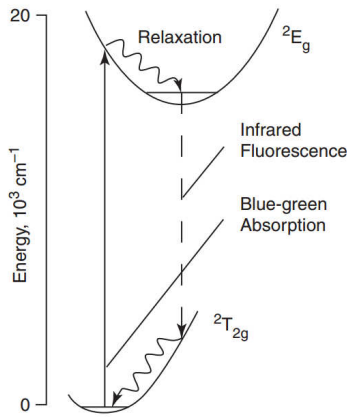


**Fig. 2.7:** Energy level structure of Ti:Sapphire. Adapted from [2].

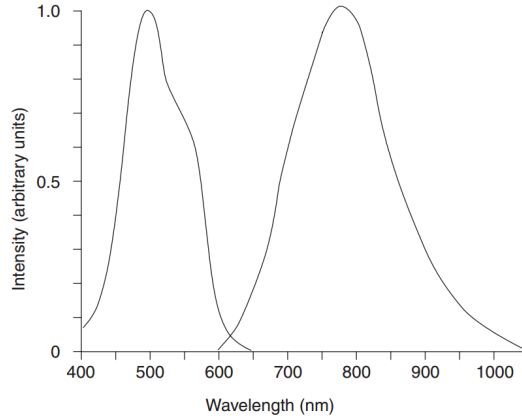


**Fig. 2.8:** Absorption and emission spectra of Ti:Sapphire. Adapted from [2].

As shown in fig. [2.8] the absorption occurs over wavelengths of 400 nm to 600 nm and the emission from 600 nm to over 1000 nm.

Due to the overlap of the absorption and emission spectrum, lasing is only possible for wavelengths longer than 670 nm. The wide spectrum is necessary to produce and amplify ultrashort pulses.

The basic principle of generating these pulses is shown in fig. [2.9].

Due to self-focusing of intense laser pulses the peak power of the pulse has to be limited when the pulse is going through material. Chirped Pulse Amplification (CPA)



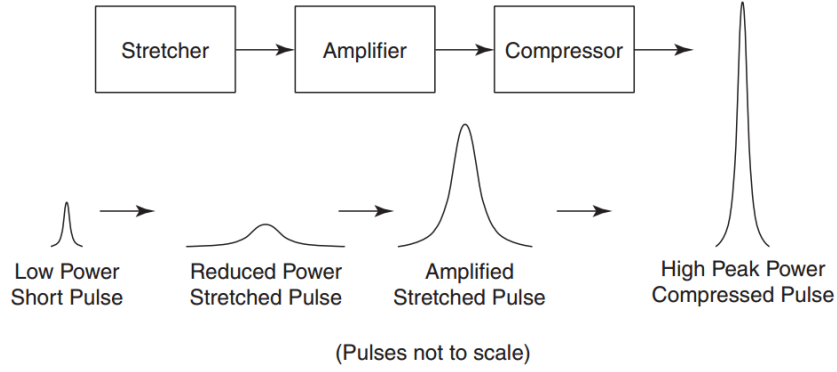


**Fig. 2.9:** Principle of chirped pulse amplification (CPA). The pulse is first stretched to decrease the peak intensity, then amplified and afterwards compressed to its original pulse duration. Adapted from [2].

is using this limited peak power to produce ultrashort pulses. CPA is done in three steps. At first the pulse is stretched, so the pulse duration increases and the peak power decreases. The longer pulse is now amplified and afterwards re-compressed to its original pulse duration.

### 2.3.2 Pulse Duration Measurements

The following section is about the measurement of the pulse duration. For energy and spectrum measurements see [6].

To measure the pulse duration of a pulsed laser several techniques can be used. This section will be limited to cross and auto correlation. For other techniques such as SPIDER (Spectral Phase Interferometry for Direct Electric-field Reconstruction) or FROG (Frequency Resolved Optical Gratings) see [7] chapter 9.4.

In general, for measuring pulse durations, shorter time scales have to be used for measurements. A photodiode can not be used for measuring femtosecond pulse durations, because its time resolution is not fast enough. All optical methods are the only way to achieve this time resolution.

Cross and auto correlation are such all optical methods and are based on the same principles. The experimental setup is similar to a Michelson interferometer (see fig. [2.10]).

The incoming beam is split up into two parts and are reunited in a nonlinear crystal to produce a sum frequency. One part of the split beam is delayed by the time  $\Delta\tau$  (see fig. [2.11]). The intensity of the generated beam is dependent on the temporal and spatial overlap of the two beam parts. As the spatial overlap is constant, the temporal overlap can be changed by moving the delay stage. The generated beam is detected with a photodiode. The intensity of it is measured dependent on the time delay (see fig. [2.12]). The resulting signal is a Gaussian function, which FWHM

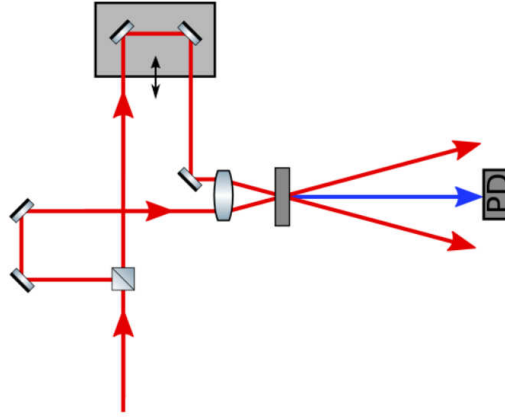


**Fig. 2.10:** Schematic setup of an optical auto correlator. The beam is split into two equal parts. One of it is delayed by the time  $\Delta\tau$  by a linear stage. In a lense the beam parts are focused in a non linear crystal to produce a sum frequency which is detected by a photodiode.

$\Delta t_2$  is determined to get the pulse duration of the incoming pulses  $\Delta t$ .

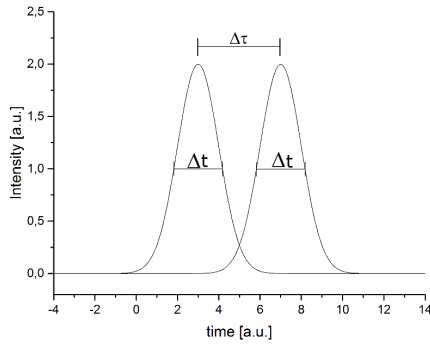


**Fig. 2.11:** Two Gaussian pulses with a time delay  $\Delta\tau$ .

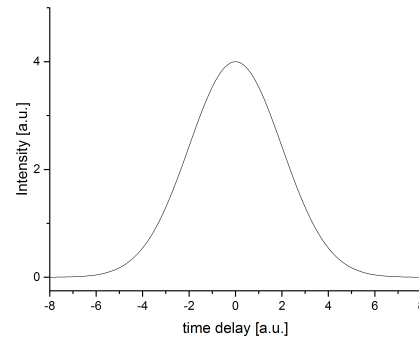


**Fig. 2.12:** Convolution signal of two Gaussian pulses dependent on the time delay  $\Delta\tau$ .

In an autocorrelation the pulses which are united in the crystal are at the same wavelength and intensity whereas in a cross-correlation they are not.

Mathematically, a cross correlation is the convolution of two signals  $f$  and  $g$ :

$$(f * g)(\tau) = \int_{-\infty}^{\infty} f^*(t)g(t + \tau)dt, \quad (2.28)$$

where  $f^*$  is the complex conjugate of  $f$  and  $\tau$  is the delay. For zero delay the resulting signal is at a maximum. At the application to intensity cross correlation the signals  $f$  and  $g$  are the intensities of the pulses. The interaction section of the two pulses in a non linear crystal and the quantities used for further discussion are shown in fig. [2.13]. The quantity  $\Delta x_0$  is related to the time delay  $\Delta\tau$  by :

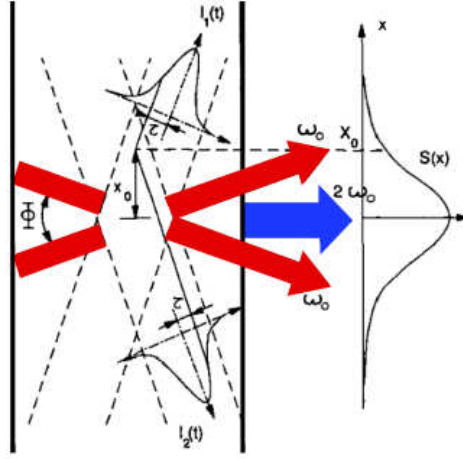


**Fig. 2.13:** Interaction of two spatially overlapped beams in a non linear crystal. Adapted from [10], slightly modified by adding color.

$$\Delta x_0 = \frac{c\Delta\tau}{2n \sin(\phi/2)}, \quad (2.29)$$

where  $n$  is the index of the crystal and  $\phi$  the angle between the beams. With these quantities the FWHM  $\Delta t$  of the incoming pulse can be determined by

$$\Delta t = K\delta_0 \frac{\Delta\tau}{\Delta x_0}, \quad (2.30)$$

where  $\delta_0$  the FWHM of the signal. [10]

## 2.4 Molecular Physics Basics

This section is about the basic knowledge of molecules, REMPI measurements and the behavior of molecules in electric fields. For a more detailed discussion, see [8] and [11].

### 2.4.1 Quantum States of Molecules

Molecules, as well as atoms, are specified by energy eigenstates. While atoms only have electronic states, molecular energy states are more complex due to rotational and vibrational eigenstates. Fig. [2.14] shows the schematic energy states in a molecule which consists of two atoms.

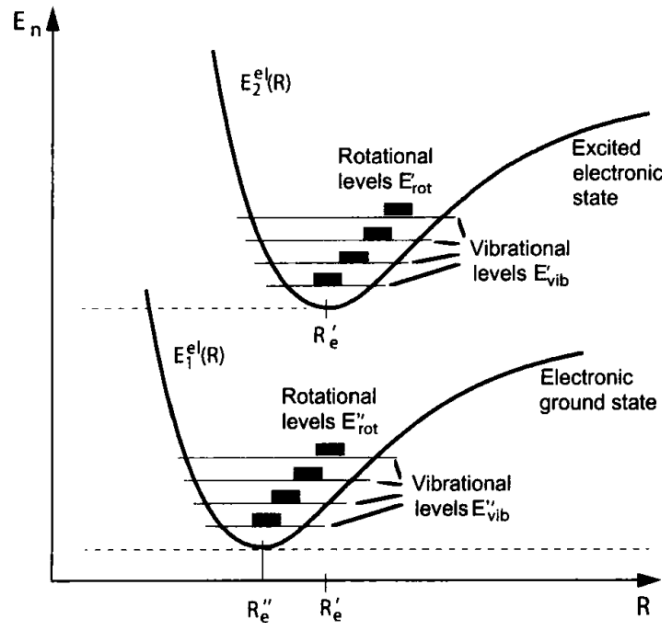


**Fig. 2.14:** Schematic energy states in a molecule which consists of two atoms. Adapted from [8].

The electronic transition energy is higher than the vibrational or rotational transition energy. The rotational transition energy is the lowest. Electronic transition is in the UV to near IR range ( $\lambda = 0.1 - 2 \mu\text{m}$ ), vibrational transitions are in the IR region ( $2 - 20 \mu\text{m}$ ) and rotational transition in the microwave range ( $1 \text{ mm} - 1 \text{ m}$ ), see fig. [2.14].

From rotational spectra the geometry of the molecule can be determined, from the vibrational spectra the forces between the atoms and from the electronic spectra the electronic states, the stability and the electron density can be determined [8].

### 2.4.2 REMPI Measurements of Molecules

REMPI (resonance-enhanced multiphoton ionization) is a technique to ionize molecules by laser pulses. The incoming photons do not have enough energy to ionize the molecule directly. Therefore, more than one photon is needed. The enhancement of this ionization is the excitation to intermediate states, which can have a long lifetime, so that even low laser intensities are sufficient for getting ion signals at resonant wavelengths. Fig. [2.15] shows three types of REMPI. The photons can have all the same energy (see (a) and (b) in fig. [2.15]) or the ionization can be achieved by a multicolor excitation (c), meaning the photons responsible for ionization have different wavelengths.

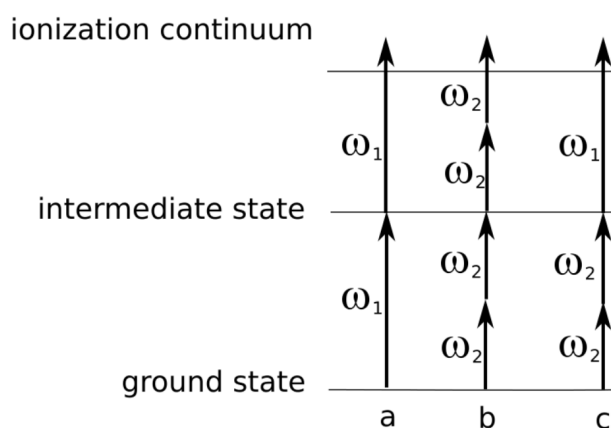


**Fig. 2.15:** Schematic overview of different REMPI types. a.) (1+1) one color REMPI, b.) (3+1) one color REMPI, c.) (2+1) two colors REMPI.

The ionized molecules can be detected by mass spectroscopy techniques (e.g. TOF-MS).

### 2.4.3 Mass Spectroscopy

There are several techniques available to detect molecules by using mass spectroscopy. The following section will be limited to time of flight (TOF) mass spectroscopy. For other techniques see [8], chapter 12.6.

In an electric field ions (e.g. produced by REMPI) are accelerated due to their charge. Their energy  $E_{\text{el}}$  is

$$E_{\text{el}} = q \cdot U, \quad (2.31)$$

with  $q$  the charge and  $U$  the voltage. Equalizing the electric energy to the kinetic energy results in the following equation

$$q \cdot U = \frac{1}{2}mv^2, \quad (2.32)$$

with  $m$  as the molecular mass and  $v$  its velocity. Due to the different masses of the molecule and its fragments, they have a different velocity and are therefore detected at different times at the multichannel plate (MCP) as illustrated in fig. [2.16].

Solving eq. [2.32] for the time  $t$  the molecules travel to the MCP, one gets

$$t(m) = \sqrt{\frac{1}{2} \frac{ms^2}{qU}}, \quad (2.33)$$

where  $s$  is the distance of acceleration.

Since every value is constant except from  $m$  and  $q$ , the following proportionality is given:

$$t \propto \sqrt{\frac{m}{q}}. \quad (2.34)$$

The time of flight is therefore dependent on the mass to charge ratio. With the measured time of flight it is now possible to get the mass to charge ratio of the molecules and the fragments.

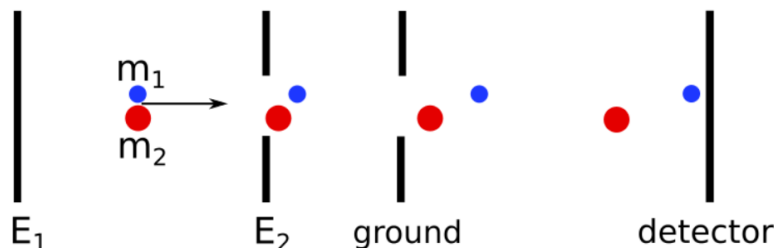


**Fig. 2.16:** Schematic setup of a time of flight mass spectrometry measurement. Two masses ( $m_1 < m_2$ ) are ionized and accelerated in an electric field due to their charge, which is equal for both. Because of their different masses, their velocity varies and they are detected at different times at the detector.

To get a higher resolution, the mass spectrometer can be modified as shown by Wiley and McLaren. When the ionization happens inside the electric field, the dependence on the ionization position can be minimized by using two voltages [12], as shown in fig. [2.16].

#### 2.4.4 Molecules in External Electric Fields

Even if a molecule is uncharged, there can be a permanent electric dipole moment which occurs due to the asymmetric density distribution of the electrons. In this case, the molecule is called polar. Molecules which have an inversion center can not be polar.

In external electric fields, an electric dipole moment is induced to polar and unpolar

molecules. The induced moment is

$$\mu_{\text{ind}}^{\text{el}} = -\alpha\epsilon, \quad (2.35)$$

where  $\alpha$  is the electric polarizability of the molecule, which is the property to shift the electrons with respect to the positive nuclei and  $\epsilon$  is the electric field. The energy  $E$  of an electric dipole moment in the electric field is

$$E = -\mu^{\text{el}}\epsilon, \quad (2.36)$$

where  $\epsilon = |\epsilon|$ . The energy for induced dipole moments is then proportional to  $|\epsilon|^2$ . The projection of the molecule-fixed dipole moment onto the electric field axis is the effective dipole moment  $\mu_{\text{eff}}$ . It is the slope of the Stark curve for an individual state:

$$\mu_{\text{eff}} = -\frac{dE}{d\epsilon}. \quad (2.37)$$

The force exerted by an electric field on a polar molecule is

$$\mathbf{F} = \mu_{\text{eff}}(\epsilon)\nabla\epsilon. \quad (2.38)$$

There are two types of states which behave different in weak electric fields: high-field and low-field seeking states [13]. In strong fields, almost every state is high-field seeking in order to minimize their energy by being attracted to the field.

With the Stark effect it is possible to separate molecules with different effective dipole moments, such as conformers [14] or rotational states [15].

### 2.4.5 Indole

Indole ( $\text{C}_8\text{H}_7\text{N}$ ) consists of a pyrrole and benzene moiety, which are sharing one bond. The mass of indole is 117 amu, it is a solid at room temperature and the melting point is at  $52^\circ\text{C}$  [20]. The structure of indole is shown in fig. [2.17].

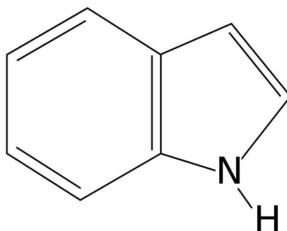


**Fig. 2.17:** Structure of Indole ( $\text{C}_8\text{H}_7\text{N}$ ).

Indole is a part of the amino acid tryptophan and is the precursor of the neurotransmitter serotonin. The emission properties of tryptophan are used in fluorescence experiments on proteins. Indole is one of the most important biological chromophores and responsible for the ability of tryptophan to absorb light around 300 nm [3]. Therefore, indole is at great interest [4].

The geometry of indole was found to be planar in the electronically ground state [16]. The dipole moment in the ground state is determined to be 1.963 D [17]. The ionization energy of indole is 7.76 eV (159 nm) [5].

Fig. [2.18] shows the absorption spectrum of indole in the UV region. With 266 nm pulses, the  $^1L_a$  state is populated with a higher probability than the  $^1L_b$  state.  $^1L_a$  and  $^1L_b$  are the lowest electronically excited states in indole and the naming of these states follows the nomenclature of Platt [18].

$^1L_a$  and  $^1L_b$  differ in their electronic density distribution. The electrons are excited to different orbitals and therefore, the properties of the molecule is different for these two states [3].

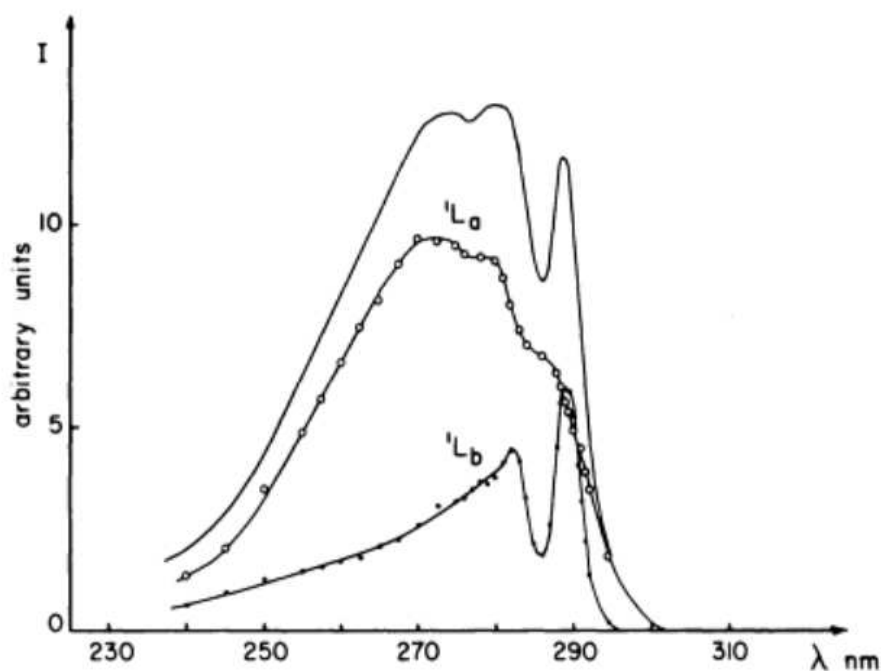


**Fig. 2.18:** Resolution of the absorption spectrum of indole. Adapted from [21].



The following figure shows the energy of different quantum states of indole in strong electric fields. For the simulation of this Stark curves molecular constants and the effective dipole moments for different states have to be known. This knowledge can be taken from rotational spectroscopy. The simulations are done with the CMIs Stark software package [25].

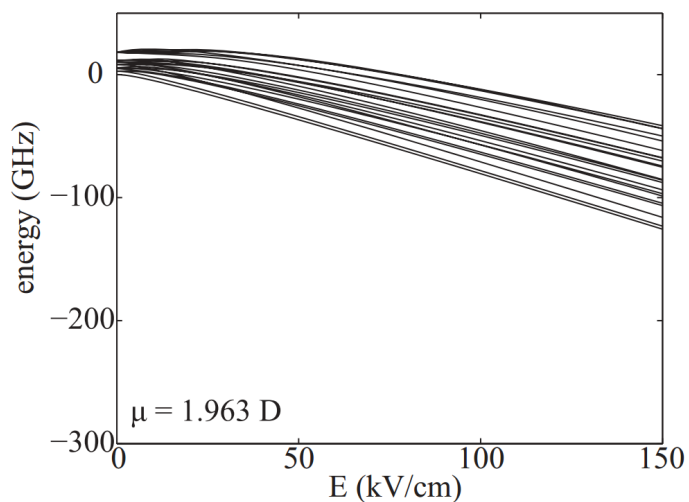


**Fig. 2.19:** Stark curves for indole. Adapted from [19].



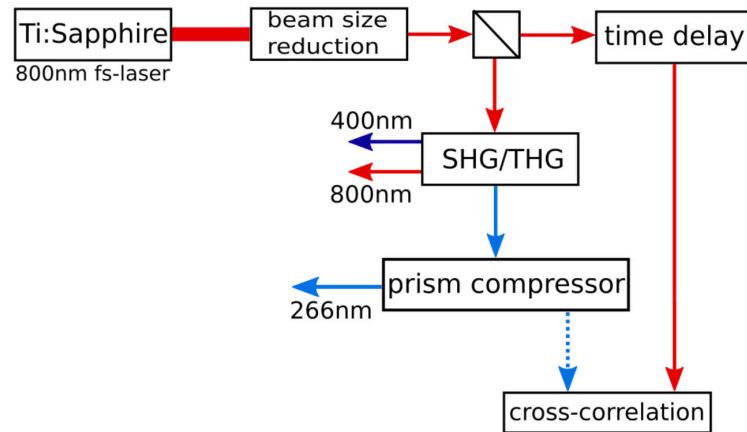
# Chapter 3

## Experimental Setup

### 3.1 Mobile Setup to Generate and Characterize UV Pulses

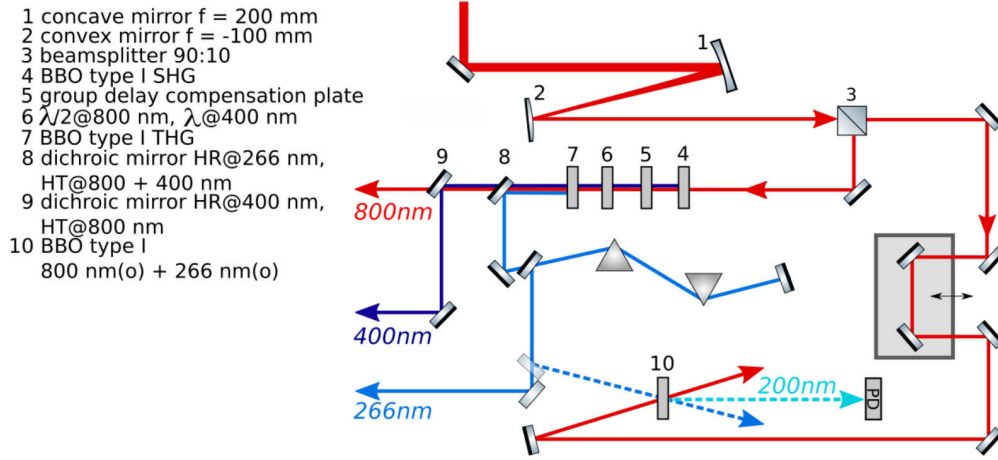
For the generation and characterization of ultrashort UV laser pulses a mobile setup option is chosen. All components are mounted on a 45 cm  $\times$  60 cm breadboard, so the setup is not fixed to a certain place in the laboratory and can be moved if necessary.

Fig. [3.1] shows the schematic overview of the setup. Starting point is a fs Ti:Sapphire laser with a central wavelength of 800 nm, a bandwidth of 60 nm and a pulse duration of 39 fs. A beam size reduction with a factor of 2 is done and 90 % of the beam energy is used for second and third harmonic generation, whereas 10 % are used for the cross correlation. The third harmonic (266 nm) is passing a prism compressor and afterwards can be coupled out towards the experiment or is characterized by the cross correlation.



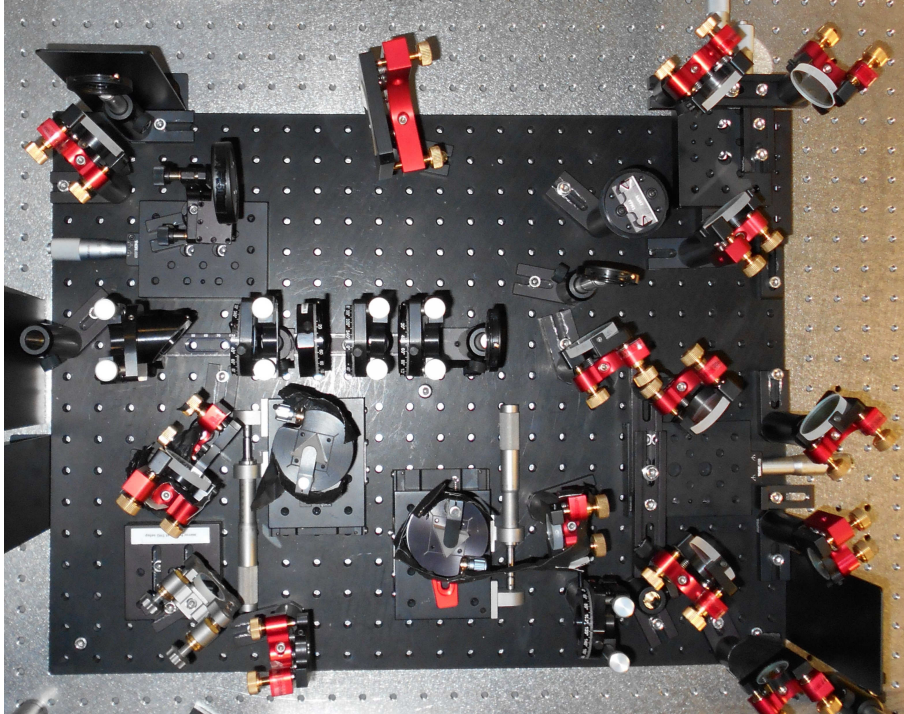
**Fig. 3.1:** Schematic overview of the setup for generating and characterizing ultrashort UV laser pulses.

Fig. [3.2] shows the setup with the elementary optical elements.



**Fig. 3.2:** Setup for generating and characterizing ultrashort UV laser pulses.

The following figure shows a photograph of the setup. Additional mirrors are placed into the fundamental beampath to ensure the temporal overlap of the pulses at the BBO for cross correlation (no. 10 in fig. [3.2]). Additionally, a second linear stage is built into the fundamental beam path (see fig. [3.3] on the upper right).



**Fig. 3.3:** Photograph of the setup to generate and characterize ultrashort UV laser pulses.

### 3.1.1 Second and Third Harmonic Generation

To generate the second and third harmonic of the Ti:Sapphire beam, a femtokit by EksmaOptics is used. The kit consists of two waveplates, two BBO-crystals (type I), a Calcite plate (CP) and three harmonic separator mirrors. Due to GVD, the thickness of the crystals is chosen by the pulse duration of the fundamental. The thickness of the crystals which are used is 0.1 mm. The setup is shown in fig. [3.4].

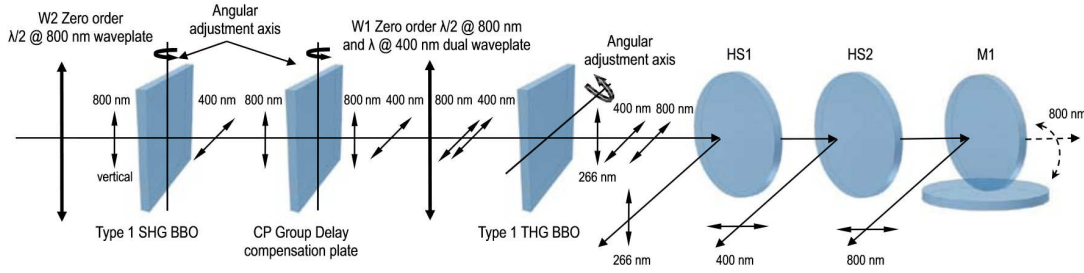


**Fig. 3.4:** Schematic overview of the components for second and third harmonic generation. The small arrows show the polarization of the light. Adapted from [26].

The fundamental beam enters the setup and is linear polarized. The first waveplate ( $\lambda/2$  at 800 nm) ensures vertical polarization of the fundamental. In the first BBO the second harmonic is generated whose polarization is orthogonal to the fundamental polarization. After the BBO both beams enter a CP plate which compensates group velocity dispersion. A second waveplate ( $\lambda/2$  at 800 nm and  $\lambda$  at 400 nm) changes the polarization of the fundamental to horizontal because both BBOs are type I and the incoming mixing photons have to have the same polarization. In the BBO for THG, the third harmonic is generated. The harmonic separators separate the wavelengths so all of them can be used separately.

The setup for THG was built  $90^\circ$  turned in polarization, so that the incoming 800 nm fundamental is horizontal polarized as well as the out coming 266 nm third harmonic, because the prism compressor needs horizontal polarized light to minimize energy loss at the surfaces.

### 3.1.2 Prism Compressor

In this setup a prism compressor of two prisms and a mirror by Newport is used. In this setup a prism compressor of two prisms and a mirror by Newport is used.

The prism compressor has been shown in 2.1.5. With eq. [2.20] the distance between the two prisms is determined to be 11 cm. The beam was coupled out under the incoming beam so that a change of height appeared in the setup, which is corrected after the setup while aligning the beam trough the detection chamber of the molecular beam machine for the measurements of indole.

### 3.1.3 Cross Correlation

To measure the pulse duration of the third harmonic, a cross-correlation is used. Therefore, the fundamental beam, which was split up earlier, is crossed in a BBO (type I,  $800\text{ (o)} + 266\text{ (o)} = 199.6\text{ (e)}$ ) with the third harmonic beam. The fourth harmonic ( $200\text{ nm}$ ) is generated and detected with a photodiode. To generate a time overlap, a delay stage is built into the beampath of the fundamental.

## 3.2 Molecular Beam Machine for TOF Mass Spectroscopy

A schematic overview of the molecular beam machine which is used for the TOF REMPI measurements is shown in fig. [3.5].

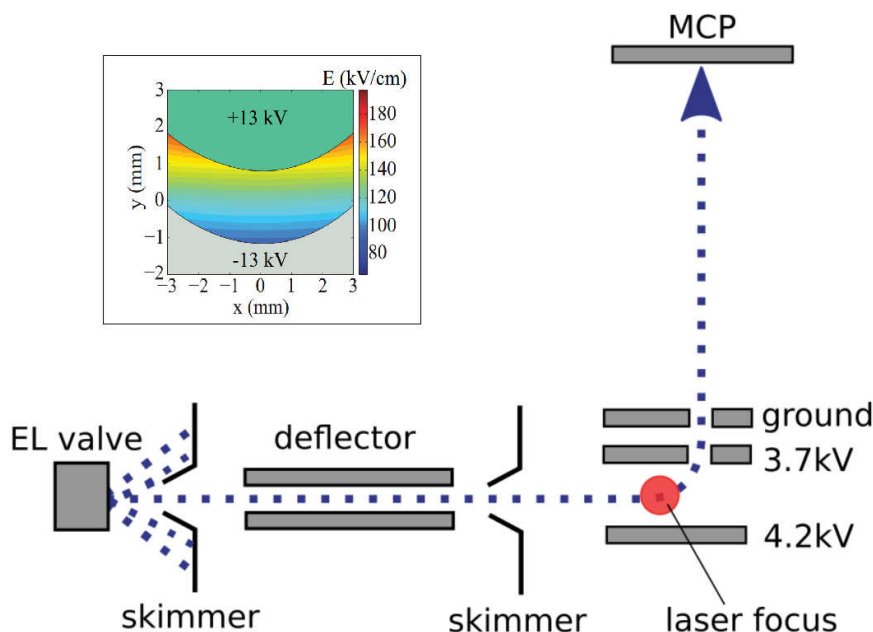


**Fig. 3.5:** Schematic overview of the molecular beam machine. The molecules leave the pulsed EL valve and are collimated by a skimmer before passing the electric field introduced by the deflector. After passing a second skimmer, the molecular beam is crossing the laser focus, which is ionizing the molecules so that they are accelerated in the electric field introduced by the TOF plates. They are finally detected at the MCP. The inset (adapted from [19]) shows a cut through the deflector and a contour plot of the electric field strength for an applied voltage of 26 kV.

The sample is inside a heatable, pulsed EL (Even Lavie)-valve. To bring the molecules into gas phase and cool them to very low temperatures, the molecules expand together with 60 bar Helium into a vacuum. The expanding molecular beam is collimated by a skimmer. The molecules enter the deflector chamber afterwards and travel through a second skimmer to enter the detection chamber. There, a focused

laser beam crosses the molecular beam to ionize the molecules. Between the TOF plates, the ionized molecules are accelerated due to their charge. They are diverted towards a micro channel plate (MCP), where the molecules are detected [19].





# Chapter 4

## Results and Discussion

### 4.1 Second and Third Harmonic Generation

For the characterization of the second and third harmonic, the spectrum and the energy are measured dependent on the incoming energy of the fundamental beam. The spectrum is taken with a spectrometer by Avantes.

Fig. [4.1] shows the spectrum of the beam after the BBO for THG with the fundamental wavelength and the generated second and third harmonic.

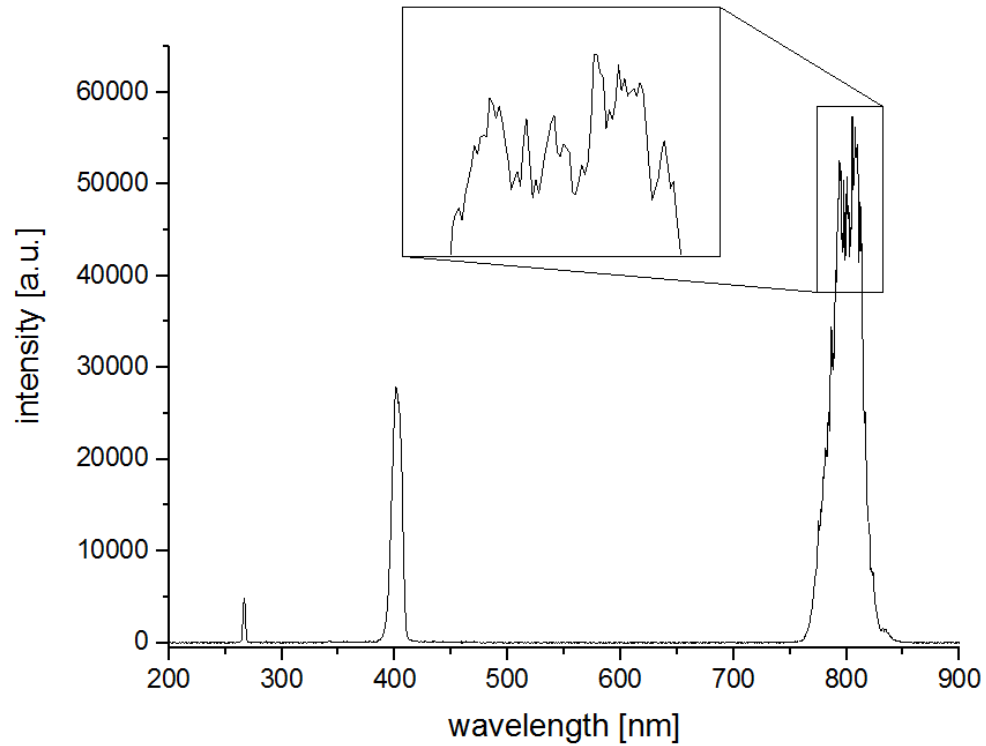


**Fig. 4.1:** Spectrum after the BBO for THG. The three wavelengths of the fundamental and second and third harmonic are present. In the spectrum of the fundamental is a dip at the main wavelength (see inset). This is the part of the photons which is taken to generate the second and third harmonic.

The fundamental has a central wavelength at 800 nm. The dip in the fundamental spectrum (see inset of fig. [4.1]) is caused by the missing photons which are taken to produce the second and the third harmonic.

The second harmonic has its maximum of intensity at 401.9 nm and the third harmonic at 266.8 nm.

After the prism compressor the spectrum only consists of the third harmonic. The part of the spectrum with the third harmonic is shown in fig. [4.2].

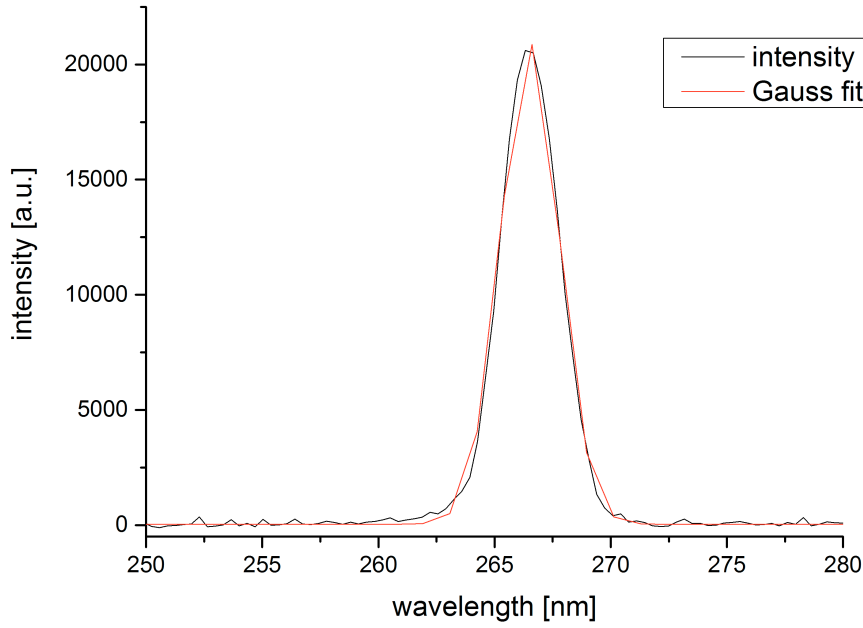


**Fig. 4.2:** Relevant part of the spectrum after the prism compressor. The central wavelength is 266.5 nm and FWHM is about 3 nm. The red line is the Gaussian fit function.

With the spectrum of the third harmonic the theoretical minimum of the pulse duration can be determined (see ch. [2.1.2]). For comparison the minimum pulse duration is determined before and after the prism compressor. Taking a Gaussian pulse shape, the following values can be determined:

|                 | before prism compressor | after prism compressor |
|-----------------|-------------------------|------------------------|
| wavelength [nm] | $266.76 \pm 0.01$       | $266.52 \pm 0.01$      |
| FWHM [nm]       | $2.53 \pm 0.01$         | $2.94 \pm 0.02$        |

With the Gaussian factor  $K = 0.441$  and the following equation

$$\Delta t \geq \frac{\lambda^2}{\Delta \lambda \cdot c} \cdot K, \quad (4.1)$$

the minimum pulse duration is determined to be  $(41.31 \pm 0.16)$  fs before the prism compressor and  $(35.51 \pm 0.24)$  fs afterwards. The measurement of the pulse duration of the third harmonic is discussed in chapter [4.2].

The theoretical pulse compression in the prism compressor occurs due to non linear effects, which broaden the spectrum of the pulse. The intensity is high enough to produce color centers in the prisms. The path of the beam inside the prism occurs red. Theoretically, this effect should not occur, because it is the opposite of pulse compression.

The theoretical pulse duration of 35 fs after the prism compressor is a good value, though, compared to the incoming fundamental with a pulsed duration of 39 fs (see ch. [4.2]).

Additionally, the energy of the third harmonic after the prism compressor is measured dependent on the incoming energy of the fundamental in front of the BBO for SHG. Fig. [4.3] shows the result.

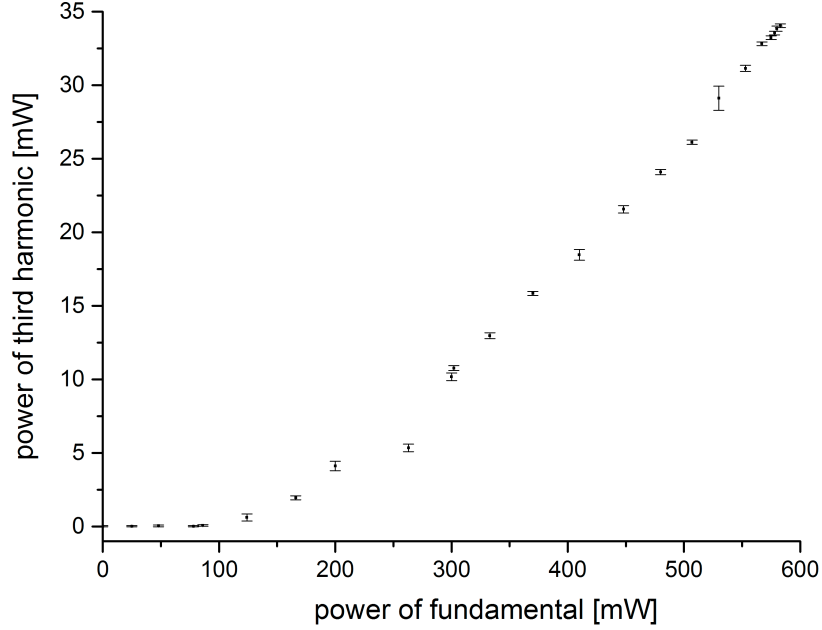


**Fig. 4.3:** Power of the third harmonic after the prism compressor dependent on the incoming power of the fundamental before the BBO for SHG.

The maximum power which can be used for THG is 585 mW and the resulting third harmonic power is 34 mW.

At the maximum power of the fundamental, an efficiency of 6 % is achieved. The energy conversion efficiency of producing the third harmonic is shown in fig. [4.4]. From 100 mW to 300 mW incoming fundamental power the conversion efficiency increases rapidly and then shows linear dependence.

The achievement of 6 % energy conversion efficiency is a good value, while considering losses at the prism compressor, and having a very thin BBO crystal due to

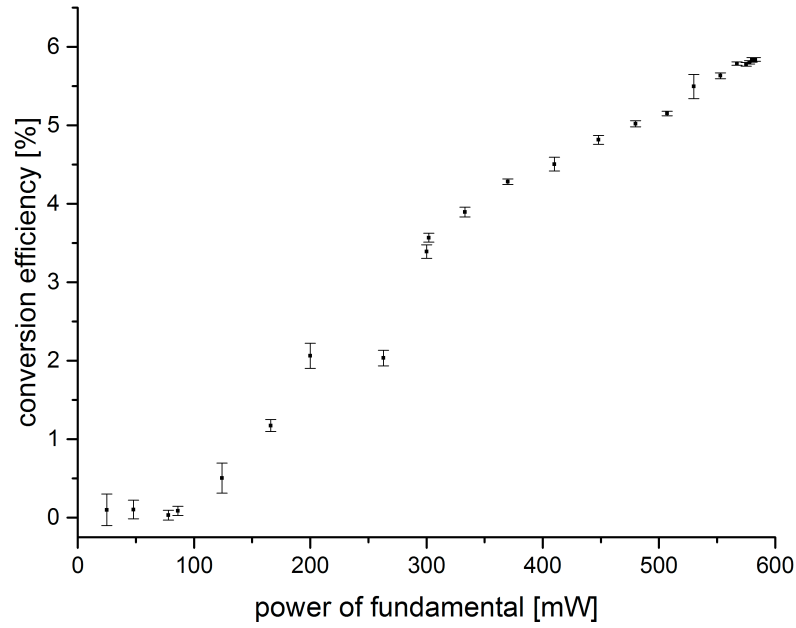


**Fig. 4.4:** Conversion efficiency of generating the third harmonic dependent on the incoming fundamental power. There is a great increase up to 300 mW. For higher fundamental powers, the efficiency increases linearly.

the short pulse duration.

The conversion efficiency at higher incoming fundamental powers could not be measured because of the limited incoming power at this setup place.

## 4.2 Auto and Cross Correlation

The pulse duration of the incoming 800 nm pulses are measured with the auto correlator 'PulseCheck' by APE. At the optimized compression which is also used for the TOF measurements (see ch. 4.3) the pulse duration is 39 fs.

The output pulse duration of the Ti:Sapphire laser is 35 fs. Between the laser output and the setup for THG, where the pulse duration is measured, the pulses travel through air and two beamsplitters, which broadens the pulse duration (see Pulse Propagation of a Light Pulse in a Transparent Medium [2.1.3]). By changing the compression at the laser, the pulses can be negatively chirped, so that the positive chirp on the travel path is compensated.

For measuring the pulse duration of the generated UV pulses, a cross correlation is planned. The spatial overlap of the two pulses has been achieved, but no temporal overlap of the pulses and therefore no signal of the fourth harmonic, which would be generated in the BBO crystal, is found.

There is a technique to determine the temporal overlap with an accuracy of one picosecond by generating plasma with one beam and scatter the second beam. If the temporal overlap is achieved, a shadow appears in the beam after the plasma. The resolution of a picosecond is achieved, because plasma in air has a life time on a picosecond time scale [27]. One picosecond temporal overlap means to have a difference in the path lengths the pulses travel of 0.3 mm.

The plasma is produced by focusing the 800 nm beam. The setup was changed to have the beams entering the lens, which focuses the beam, collinear. The scattering of the 266 nm beam could not be seen at the 800 nm plasma while moving the linear stage. It is possible to produce a plasma even with the 266 nm beam at 35 mW. Scattering the 800 nm beam at the 266 nm plasma gives no result, neither.

The temporal overlap of the pulses is not achieved in this thesis and therefore, the pulse duration of the generated third harmonic is unknown.

## 4.3 Fragmentation of Indole

### 4.3.1 Fragmentation at 800 nm pulses

The first TOF REMPI mass spectra are taken with 800 nm laser pulses. Fig. [4.5] shows a TOF mass spectrum at the settings shown in the following table.

|                      |                 |
|----------------------|-----------------|
| detector voltage     | 5 kV            |
| TOF voltage 1        | 4.2 kV          |
| TOF voltage 2        | 3.7 kV          |
| laser wavelength     | 800 nm          |
| laser energy         | 250 $\mu$ J     |
| pulse duration       | 39 fs           |
| molecule             | indole          |
| valve temperature    | 60°C            |
| valve laser delay    | 620 $\mu$ s     |
| valve pulse duration | 12.5 $\mu$ s    |
| repetition rate      | 50 Hz           |
| backing gas          | Helium (60 bar) |

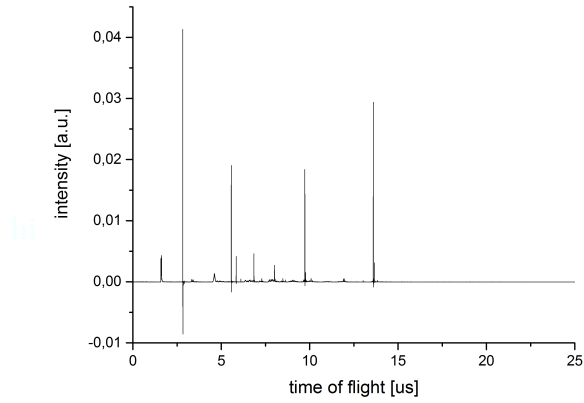


**Fig. 4.5:** Time of flight mass spectrum.

Different fragments are detected at the MCP at different times due to their mass. A conversion from the time of flight to mass to charge ratio is done by knowing two peaks: The peak of the parent ion indole (mass 117 amu) at 13.6  $\mu$ s and the peak of the backing gas helium (mass 4 amu) at 2.83  $\mu$ s. By knowing these values, the  $x$ -axis can be calibrated with:

$$\frac{m}{q} = c \cdot (t - t_{\text{off}})^2, \quad (4.2)$$

where  $m$  is the mass with  $[m] = \text{amu}$ ,  $q$  the charge with  $q = ne$  for  $n \in \mathbb{N}$ ,  $c$  a constant with  $[c] = \frac{\text{amu}}{e \cdot \mu\text{s}^2}$  (see ch. [2.4.3]) and  $t$  the time of flight with  $[t] = \mu\text{s}$ .

$t_{\text{off}}$  can be determined by

$$t_{\text{off}} = \frac{\sqrt{\frac{m_1}{m_2}} \cdot t_2 - t_1}{\sqrt{\frac{m_1}{m_2}} - 1}. \quad (4.3)$$

For the measurements with 800 nm, the calibration formula is

$$\frac{m}{q} = 0.6705 \cdot (t - 0.39)^2 \quad (4.4)$$

The TOF trace then is the intensity dependent on the mass to charge ratio (see fig. [4.6]). Fig. [4.7] shows in detail the red marked box from fig. [4.6].

hi

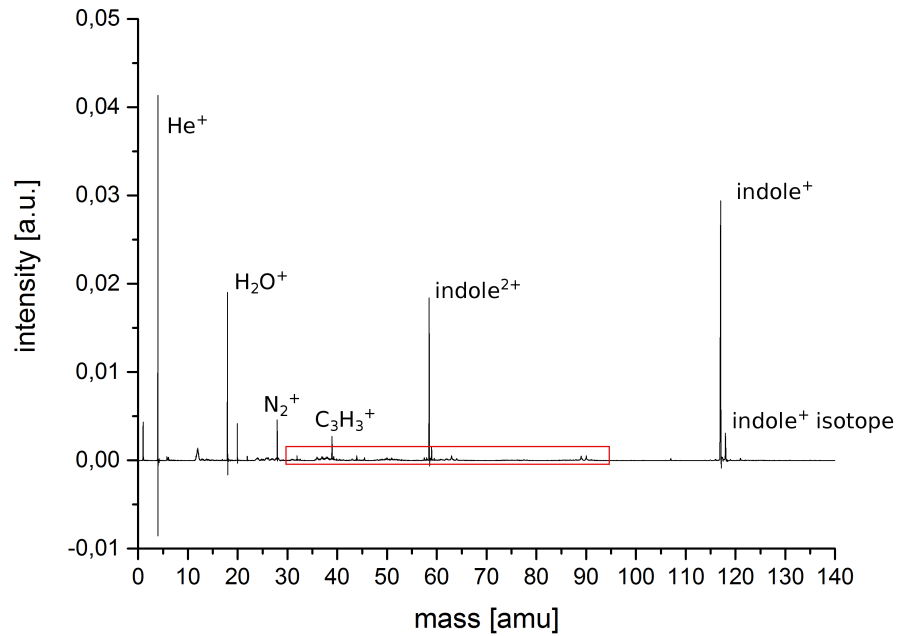


**Fig. 4.6:** TOF measurement at 250  $\mu\text{J}$  with 800 nm laser pulses. The red box is shown in the next figure in more detail.

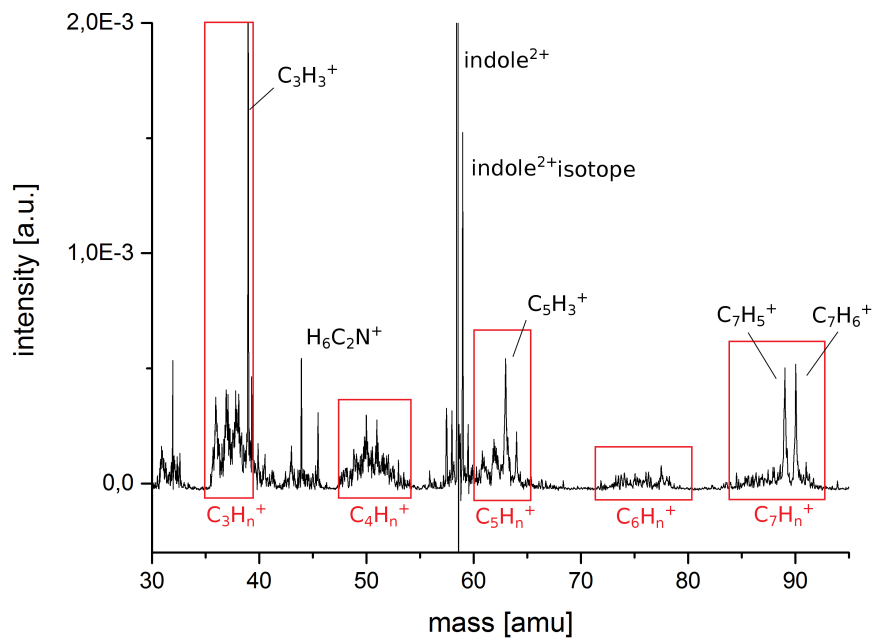


**Fig. 4.7:** TOF trace in more detail. Most of the masses are named in the figure itself. For further masses and the relating fragments see the table in [A.2].

Indole has a mass of 117 amu. At 118 amu an isotope of indole (isotope of hydrogen, nitrogen or carbon) is seen. At half the mass at 58.5 amu the double charged indole appears. The backing gas helium is at 4 amu.

As shown in fig. [4.7], the most appearing fragment is  $\text{C}_3\text{H}_3^+$ .

To determine, which atoms isotope is appearing in this spectrum, the natural isotope ratios of hydrogen, nitrogen and carbon are compared to the ratio of the intensity of the two peaks in the spectrum. Taking all 800 nm TOF traces into account, the ratio of indoleisotope to indole is  $(0.10379 \pm 0.05194)$ . The values of the isotopes are taken from [28], [29] and [30].

| atom            | appearance (all isotopes = 1) | ratio (isotope to non isotope) |
|-----------------|-------------------------------|--------------------------------|
| $^1\text{H}$    | 0.9998                        | 0.0001                         |
| $^2\text{D}$    | 0.0001                        |                                |
| $^{12}\text{C}$ | 0.9893                        | 0.0108                         |
| $^{13}\text{C}$ | 0.0107                        |                                |
| $^{14}\text{N}$ | 0.99636                       | 0.0037                         |
| $^{15}\text{N}$ | 0.00364                       |                                |

Due to the very low ratio of nitrogen and deuterium compared to the ratio measured in the TOFs, the isotope of indole tends to be an indole with one  $^{13}\text{C}$  atom.



### 4.3.2 Fragmentation at 269 nm pulses

TOF traces are also measured with 269 nm pulses. 269 nm are used for TOF MS instead of 266 nm pulses because of higher intensities at this wavelength. After optimizing the setup again, the maximum intensity is at 266 nm (see ch. [4.1]), the R2PI measurements are not repeated again for 266 nm pulses. Fig. [4.8] shows a TOF trace at a laser energy of 19  $\mu$ J with 269 nm pulses.

The calibration of the  $x$ -axis is done in the same way as for the 800 nm TOF traces. Indole has a time of flight of 13.545  $\mu$ s and helium of 2.8575  $\mu$ s. With eq. [4.2, 4.3] the calibration is:

$$\frac{m}{q} = 0.6805 \cdot (t - 0.433)^2. \quad (4.5)$$

Comparing the mass spectra of indole at 800 nm and 269 nm pulses, the spectrum at 269 nm shows less fragmentation and background signal as the spectrum at 800 nm does.

For further characterization and comparison of the mass spectra of indole at 800 nm and 269 nm pulses, two measurements are compared: the 800 nm 25 mW and the 269 nm 19 mW measurement due to the comparable laser power. The detector voltage as well as the TOF voltages are equal at both measurements.

The following table shows the signal intensity of indole without normalization. From both values of the signal the background is subtracted.

|               | indole <sup>+</sup> signal [a.u.] |
|---------------|-----------------------------------|
| 800 nm, 25 mW | 0.0083                            |
| 269 nm, 20 mW | 0.0129                            |

The signal of ionized indole at even lower laser intensities is higher for 269 nm pulses. All indole<sup>+</sup> signal intensities are shown in [A.3].

This higher signal occurs due to the electronic energy levels in indole. With 269 nm photons, resonant intermediate states can be excited, so the efficiency of absorbing photons is higher. For the ionization of indole by 800 nm photons, five photons are needed and no resonant intermediate states can be excited, so that at low laser intensities the efficiency of ionizing this molecule is lower.

The intermediate state, which is excited with one 269 nm photon is probably the <sup>1</sup>L<sub>a</sub> state (see ch. [2.4.5])

iii

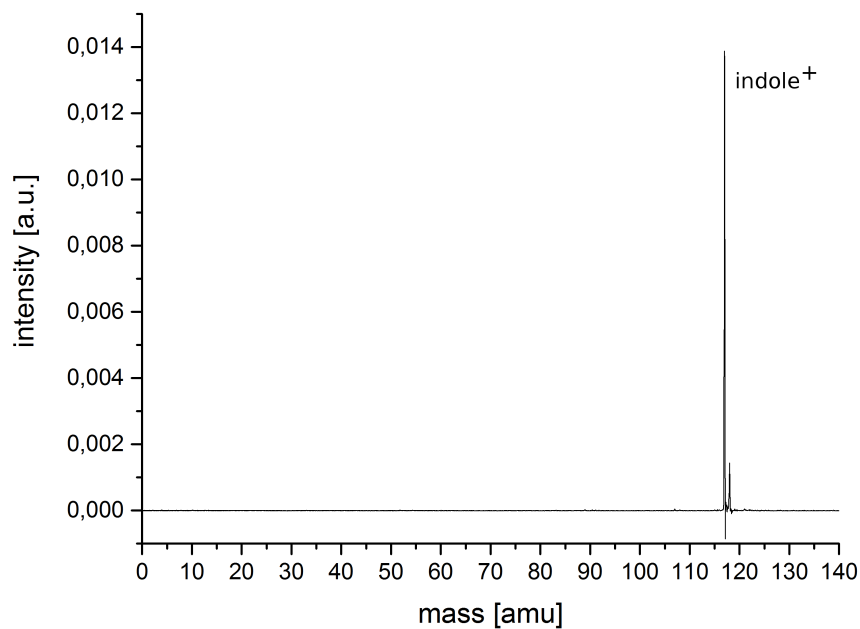


**Fig. 4.8:** TOF spectrum of the measurement with 269 nm laser pulses. Nearly no fragment is seen in this TOF spectrum. Fig. [4.9] shows the TOF spectrum in a smaller range of intensity.

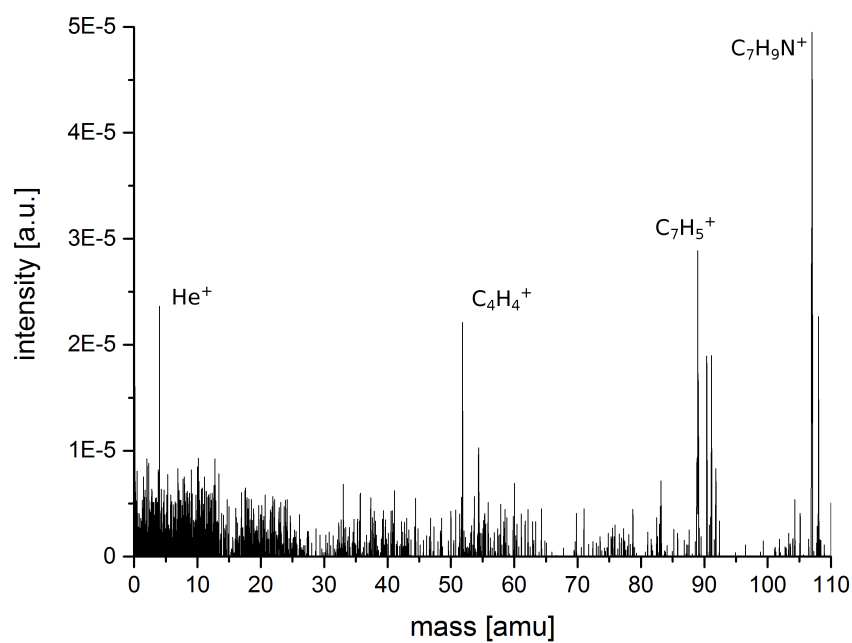


**Fig. 4.9:** TOF spectrum with 269 nm laser pulse in a smaller range of intensity.

## 4.4 Deflection of Indole

The following measurements describe the behavior of indole in a strong inhomogeneous electric field. Spatial profiles of indole are taken at different deflector voltages. Spatial profile means to scan the height of the molecular beam with respect to the laser focus. Two spatial profiles at different deflector voltages are shown in fig. [4.10]. The black curve shows the spatial profile of indole without deflector voltage, whereas the red curve shows the spatial profile at 24 kV deflector voltage. To determine the deflection, the profiles are fitted assuming a Gaussian shape and determining the maximum position for each profile. An example for the fit of a Gaussian shape to the spatial profile is shown in [A.4]. The deflection for the red curve in fig. [4.10] is 0.33 mm from the black curve.

For the deflection of indole no simulations have been done, but the deflection of 0.33 mm at a deflector voltage of 24 kV matches the magnitude from deflection profiles of indole presented in [19].

The negative deflection shown in figure [4.10] shows a deflection upwards, because the molecular beams with respect to the laser focus has to be moved downwards.

For further demonstration of the spatial deflection, the position of the maxima are taken to get the deflection dependence on the deflector voltage. The result is shown in fig. [4.11]

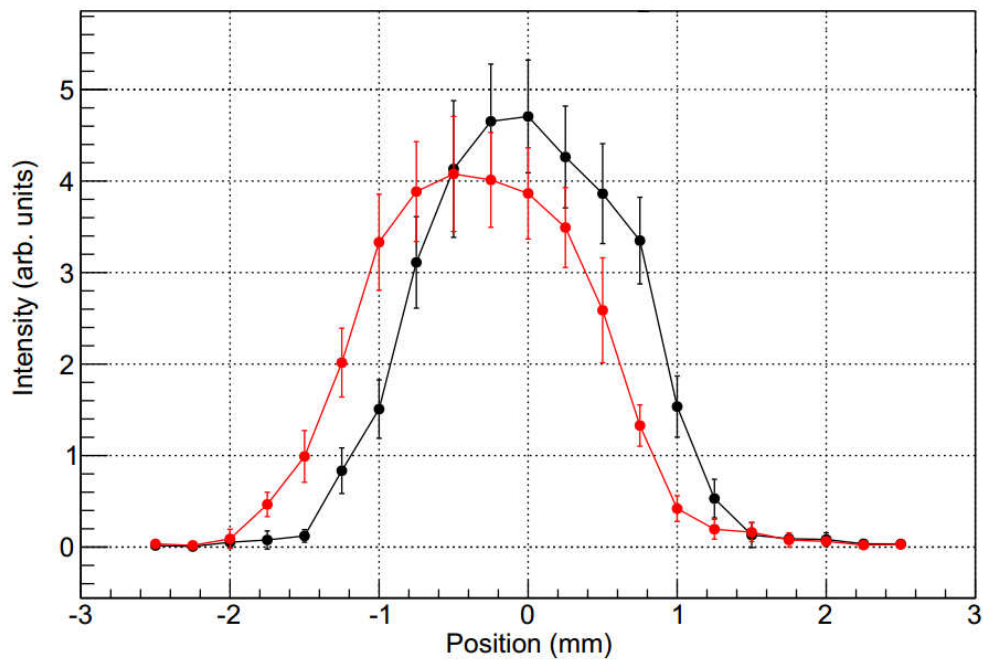


**Fig. 4.10:** Spatial profiles of indole at two different deflector voltages. The black data show the spatial profile with zero deflector voltage. The red data show the spatial profile at 24 kV deflector voltage. The deflection is 0.33 mm.

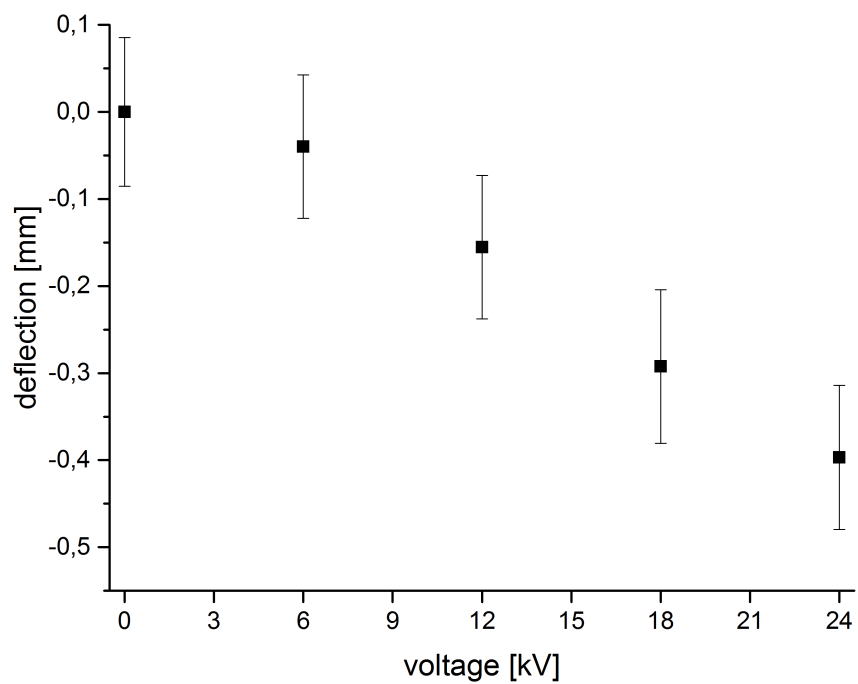


**Fig. 4.11:** Deflection profile of indole. The deflection is shown dependent on the deflector voltage. A deflection of up to 0.4 mm at 24 kV deflector voltage is measured.

# Chapter 5

## Conclusion

The aim of this thesis to generate UV pulses for R2PI measurements of indole is achieved.

With the nonlinear processes second harmonic generation and sum frequency generation UV pulses are generated from a Ti:Sapphire laser by using BBO-crystals. The central wavelength of the generated UV pulses is at 266.5 nm with a bandwidth of 2.94 nm. An energy conversion efficiency of 6 % of the fundamental energy is achieved. The maximum energy which can be used for producing UV pulses is 585  $\mu$ J and the resulting UV energy is 34  $\mu$ J.

The cross correlation which is used for measuring the pulse duration does not give a result due to the missing temporal overlap. Several techniques do not give a result, neither. The theoretical minimum pulse duration of 35 fs due to the spectrum gives positive evidence for a short pulse duration.

TOF REMPI measurements of indole are taken at 800 nm IR and 269 nm UV pulses. The mass spectra show differences in the fragmentation. When ionizing indole with UV pulses via R2PI nearly no fragmentation occurs. This gives evidence for an electronic intermediate state which is excited by these UV pulses.

Additionally, the spatial deflection of indole in electrostatic fields is measured. At an applied deflector voltage of 24 kV the spatial deflection of the molecular beam is 0.4 mm.



# Bibliography

- [1] Misra, P. (editor) : *Ultraviolet Spectroscopy and UV lasers*, Practical Spectroscopy Series, **30**, Taylor & Francis e-Library, 2005.
- [2] *Spitfire User's Manual*, 255A, Rev. A, <http://www.spectra-physics.com/documents/service/user-manuals/255A,%20Rev.%20A,%20Spitfire%20User%27s%20Manual.pdf>, abgerufen am 9. August 2015.
- [3] Montero, R. et al. : *Ultrafast Photophysics of the Isolated Indole Molecule*, J. Phys. Chem. A, 2012, **116**, 2698-2703.
- [4] Vivian JT, et al. : *Mechanisms of tryptophan fluorescence shifts in proteins*. Biophysical Journal, 2008 , **80**(5), 2093-2109.
- [5] Hager, J.W., et al. : *Two-laser photoionization supersonic jet mass spectrometry of aromatic molecules*. Anal. Chem. ,1988, **60**, 5.
- [6] C. Rullière : *Femtosecond Laser Pulses: Principles and Experiments*, Springer Verlag, 2004.
- [7] J.-C. Diels : *Ultrashort Laser Pulse Phenomena*, Academic Press, 2006.
- [8] W. Demtröder : *Molekülphysik: Theoretische Grundlagen und experimentelle Methoden*, Oldenbourg Wissenschaftsverlag, überarbeitete und erweiterte Auflage, 2013.
- [9] *Newport Prism Compressor Application Note*, <http://assets.newport.com/webDocuments-EN/images/12243.PDF>, abgerufen am 5. August 2015 .
- [10] Brun, A. et al. : *Single shot characterization of ultrashort light pulses*, J. Phys. D: Appl. Phys, **24**, 1991, 1225-1233.

- [11] Atkins, P.; Friedman, R. : *Molecular Quantum Mechanics*, 5.Auflage, 2010.
- [12] Wiley, W. C.; McLaren, I. H. : *Time-of-Flight Mass Spectrometer with Improved Resolution*, Rev. of Scientific Instruments, 1955, **26**, 12.
- [13] *Low and High Field Seeking Molecules*, <http://physics.aps.org/focus/supplement/high-low-seeking.html>, abgerufen am 30. August 2015
- [14] Filsinger, F.; et al. : *Reine Proben einzelner Konformere: die Trennung von Stereoisomeren komplexer Moleküle mittels elektrischer Felder*, Angew. Chem., 2009, **121**, 7033-7035.
- [15] Filsinger, F.; et al. : *Quantum-state selection, alignment, and orientation of large molecules using static electric and laser fields*, The Journal of Chemical Physics, **131**, 064309-1.
- [16] Suenram, R. D. ; et al. : *Microwave spectrum and  $^{14}\text{N}$  quadrupole coupling constants of indole*, J. Mol. Spectrosc., 1988, **127**, 472–480.
- [17] C. Kang; et al. : *Experimental measurement of the induced dipole moment of an isolated molecule in its ground and electronically excited states: Indole and indole-  $\text{H}_2\text{O}$* , J. Chem. Phys., 2005, **122**, 174301.
- [18] Platt, J. R., J. Chem. Phys., 1949**17**, 484.
- [19] Trippel, S. et al. : *Spatial separation of state- and size- selected neutral clusters*, Phys. Rev. A, 2012, **86**, 033202.
- [20] NIST webbook, *Indole*, <http://webbook.nist.gov/cgi/cbook.cgi?ID=C120729&Mask=400>, abgerufen am 6.9.2015.
- [21] Valeur, B. et al., Photochem. Photobiol., 1977, **25**, 441.
- [22] Ch. Brand : *Shaping and Modelling Electronically Excited States of Indoles*, Dissertation, Heinrich-Heine-Universität Düsseldorf, 2013.
- [23] Fundamentals of modern UV-VISible spectroscopy (1996) Hewlett-Packard Publication Nr. 12-5965-5123E, <http://web.uni-plovdiv.bg/plamenpenchev/mag/books/spectroscopy/PRIMER.PDF>, abgerufen am 27.08.2015



- [24] R. B. van Order, H. G Lindwall: Indole, Chem. Rev., 1941, **30**, 69-96.
- [25] Yuan-Pin Chang, Frank Filsinger, Boris G. Sartakov, Jochen Küpper, *CMIstark: Python package for the Stark-effect calculation and symmetry classification of linear, symmetric and asymmetric top wavefunctions in dc electric fields*, Computer Physics Communications, **185**, Issue 1, 2014, 339-349, ISSN 0010-4655,
- [26] <http://eksmaoptics.com/femtoline-components/femtoline-nonlinear-laser-crystals/femtokits-for-third-harmonic-generation-of-ti-sapphire-laser/>,  
abgerufen am 01.09.2015.
- [27] A. Couairon, A Mysyrowicz, Physics Reports, 2007, **441**, 47 – 189.
- [28] <http://www.webelements.com/hydrogen/isotopes.html>,  
abgerufen am 10.09.2015.
- [29] <http://www.webelements.com/nitrogen/isotopes.html>,  
abgerufen am 7.09.2015.
- [30] <http://www.webelements.com/carbon/isotopes.html>,  
abgerufen am 7.09.2015.
- [31] Küpper, J. : *Rotationsaufgelöste Laserspektroskopie von Schwingungsbanden des Indols*, Diplomarbeit, Universität Düsseldorf, 1996.
- [32] Demtröder, W. : *Laserspektroskopie 2: Experimentelle Methoden*, Springer Verlag, 2013.



# List of Figures

|      |  |    |
|------|--|----|
| 2.1  | Time evolution of the electric field in a Gaussian pulse [6]. . . . .                            | 4  |
| 2.2  | Time evolution of the electric field in a chirped Gaussian pulse [6]. . .                        | 6  |
| 2.3  | Prism compressor setup. [9] . . . . .  | 7  |
| 2.4  | Process of second harmonic generation. . . . .   | 10 |
| 2.5  | Schematic illustration of phase matching. . . . .  | 10 |
| 2.6  | Process of sum frequency generation. . . . .   | 11 |
| 2.7  | Energy level structure of Ti:Sapphire. [2] . . . . .   | 12 |
| 2.8  | Absorption and emission spectra of Ti:Sapphire. [2] . . . . .                                    | 12 |
| 2.9  | Principle of CPA. [2] . . . . .  | 13 |
| 2.10 | Schematic setup of an optical auto correlator. . . . .   | 14 |
| 2.11 | Two Gaussian pulses with a time delay $\Delta\tau$ . . . . .                                     | 14 |
| 2.12 | Convolution signal of two Gaussian pulses. . . . .   | 14 |
| 2.13 | Interaction of two spatially overlapped beams in a non linear crystal .                          | 15 |
| 2.14 | Schematic energy states in a molecule which consists of two atoms. [8]                           | 16 |
| 2.15 | Schematic overview of different REMPI types. . . . .   | 17 |
| 2.16 | Schematic setup of a time of flight mass spectroscopy measurement.                               | 18 |
| 2.17 | Structure of Indole ( $C_8H_7N$ ). . . . .   | 19 |
| 2.18 | Resolution of the absorption spectrum of indole. Adapted from [21]. .                            | 20 |
| 2.19 | Stark curves for indole. Adapted from [19]. . . . .  | 21 |
| 3.1  | Schematic overview of the Setup. . . . .   | 23 |
| 3.2  | Setup for generating and characterizing ultrashort UV laser pulses. .                            | 24 |
| 3.3  | Photograph of the setup to generate and characterize ultrashort UV<br>laser pulses. . . . .      | 24 |
| 3.4  | Schematic overview of the components for second and third harmonic<br>generation. [26] . . . . . | 25 |
| 3.5  | Schematic overview of the molecular beam machine. . . . .  | 26 |
| 4.1  | Spectrum after the BBO THG . . . . .   | 29 |
| 4.2  | Relevant part of the spectrum after the PC . . . . .   | 30 |
| 4.3  | Power of the third harmonic dependent on the incoming power of the<br>fundamental. . . . .       | 31 |

|      |   |    |
|------|---|----|
| 4.4  | Conversion efficiency of generating the third harmonic dependent on the incoming fundamental power. . . . . | 32 |
| 4.5  | Time of flight mass spectrum. . . . .   | 34 |
| 4.6  | TOF measurement at 250 $\mu$ J with 800 nm laser pulses. . . . .  | 35 |
| 4.7  | TOF trace in more detail. . . . .   | 35 |
| 4.8  | TOF spectrum of the measurement with 269 nm laser pulses. . . . .   | 38 |
| 4.9  | TOF spectrum with 269 nm laser pulse in a smaller range of intensity. . . . .                               | 38 |
| 4.10 | Spatial profiles of indole at two different deflector voltages. . . . .                                     | 40 |
| 4.11 | Deflection profile of indole. . . . .   | 40 |
| A.1  | Spatial profile fitted with Gaussian function. . . . .  | 51 |

# Appendix A

## Appendix

### A.1 Second Harmonic Generation

This section shows the mathematical description of SHG.

To show, that the second harmonic has a frequency  $2\omega_1$ , when the incoming photons have both the frequencies  $\omega_1$ , the polarization of the material is used. SHG is a second order non linear effect, so for the polarization the second term of eq. [2.25] is used. Assuming plane waves, the electric field at a certain position ( $\mathbf{r} = \mathbf{0}$ ) can be written as

$$E(\omega) = E_0 \cos(\omega t) \quad (\text{A.1})$$

The polarization is

$$\begin{aligned} \mathbf{P}^{(2)}(\omega_1) &= \epsilon_0 \chi^2 (E_0 \cos(\omega_1 t))^2 \\ &= \epsilon_0 \chi^2 E_1^2 \cos^2(\omega_1 t) \\ &= \epsilon_0 \chi^2 E_0^2 \frac{1}{2} (\cos(2\omega_1 t) + 1) \\ &= \frac{\epsilon_0 \chi^2 E_0^2 (\cos(2\omega_1 t))}{2} + \frac{\epsilon_0 \chi^2 E_0^2}{2} \end{aligned} \quad (\text{A.2})$$

The polarization consists of two terms: One is constant and represents the constant electric field part, the second describes the oscillation with the frequency  $2\omega_1$ . This oscillation is responsible for the emitted radiation with doubled frequency.

## A.2 Fragmentation of Indole

This section shows all masses of the TOF traces (800 nm and 269 nm measurements), which can be related to a certain fragment of indole or to the background signal:

| mass [g/mol] | fragments   |
|--------------|---|
| 1            | H <sup>+</sup>  |
| 4            | He <sup>+</sup>   |
| 6            | C <sup>2+</sup>   |
| 12           | C <sup>+</sup>  |
| 18           | H <sub>2</sub> O <sup>+</sup>   |
| 20           | He <sup>+</sup>   |
| 24           | C <sub>2</sub> <sup>+</sup>   |
| 25           | C <sub>2</sub> H <sup>+</sup>   |
| 26           | C <sub>2</sub> H <sub>2</sub> <sup>+</sup> or CN <sup>+</sup>               |
| 27           | HCN <sup>+</sup>  |
| 28           | H <sub>2</sub> CN <sup>+</sup> or N <sub>2</sub> <sup>+</sup>               |
| 32           | (NH <sub>2</sub> ) <sub>2</sub> <sup>+</sup> or O <sub>2</sub> <sup>+</sup> |
| 36           | C <sub>3</sub> <sup>+</sup>   |
| 37           | C <sub>3</sub> H <sup>+</sup>   |
| 38           | C <sub>3</sub> H <sub>2</sub> <sup>+</sup>                                  |
| 39           | C <sub>3</sub> H <sub>3</sub> <sup>+</sup>                                  |
| 43           | C <sub>2</sub> H <sub>5</sub> N <sup>+</sup>                                |
| 44           | C <sub>2</sub> H <sub>6</sub> N <sup>+</sup>                                |
| 49           | C <sub>4</sub> H <sup>+</sup>   |
| 50           | C <sub>4</sub> H <sub>2</sub> <sup>+</sup>                                  |
| 51           | C <sub>4</sub> H <sub>3</sub> <sup>+</sup>                                  |
| 58.5         | indole <sup>2+</sup>  |
| 59           | indoleisotope <sup>2+</sup>   |
| 61           | C <sub>5</sub> H <sup>+</sup>   |
| 62           | C <sub>5</sub> H <sub>2</sub> <sup>+</sup>                                  |
| 63           | C <sub>5</sub> H <sub>3</sub> <sup>+</sup>                                  |
| 64           | C <sub>5</sub> H <sub>4</sub> <sup>+</sup>                                  |
| 70           | C <sub>5</sub> H <sub>6</sub> N <sup>+</sup>                                |
| 71           | C <sub>5</sub> H <sub>7</sub> N <sup>+</sup>                                |
| 89           | C <sub>7</sub> H <sub>5</sub> <sup>+</sup>                                  |
| 90           | C <sub>7</sub> H <sub>6</sub> <sup>+</sup>                                  |
| 91           | C <sub>7</sub> H <sub>7</sub> <sup>+</sup>                                  |
| 107          | C <sub>7</sub> H <sub>9</sub> N <sup>+</sup>                                |
| 108          | C <sub>7</sub> H <sub>10</sub> N <sup>+</sup>                               |
| 117          | indole <sup>+</sup>   |
| 118          | indoleisotope <sup>+</sup>  |

### A.3 Indole<sup>+</sup> Signal at TOF Measurements

The following table shows the signal intensities of indole<sup>+</sup> at all TOF measurements which are taken and used for the comparison of IR to UV ionization by REMPI. The background signal was subtracted from all signals.

| wavelength | power  | indole <sup>+</sup> signal intensity [a.u.] |
|------------|--------|---|
| 800 nm     | 25 mW  | 0.0073                                      |
| 800 nm     | 50 mW  | 0.0260                                      |
| 800 nm     | 100 mW | 0.0333                                      |
| 800 nm     | 150 mW | 0.0339                                      |
| 800 nm     | 200 mW | 0.0304                                      |
| 800 nm     | 250 mW | 0.0284                                      |
| 800 nm     | 350 mW | 0.0266                                      |
| 269 nm     | 20 mW  | 0.0129                                      |
| 269 nm     | 14 mW  | 0.0092                                      |
| 269 nm     | 10 mW  | 0.0071                                      |
| 269 nm     | 7 mW   | 0.0043                                      |
| 269 nm     | 4 mW   | 0.0010                                      |

### A.4 Spatial Profiles Fit

The following figure shows the spatial profile of indole fitted with a Gaussian function. The data were taken at zero deflector voltage and 800 nm pulses with an energy of 170  $\mu$ J.

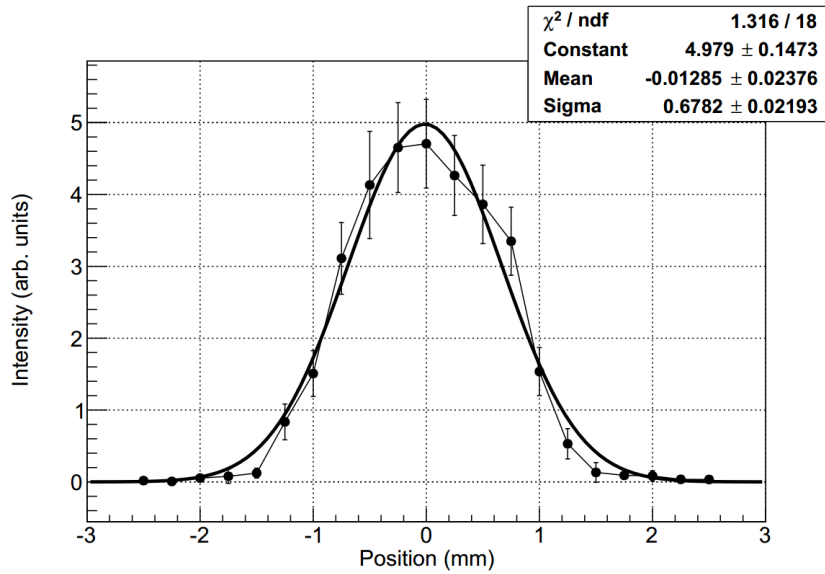


**Fig. A.1:** Spatial profile of the molecular beam at a deflector voltage of 0 kV and ionization via REMPI with 800 nm pulses and an energy of 170  $\mu$ J. To determine the deflection the data is fitted with a Gaussian function.





# Acknowledgment

At the very end of my thesis I would like to thank all those people who made this thesis possible.

First of all, I would like to thank Prof. Dr. Jochen Küpper, Dr. Daniel Horke and the group *Controlled Molecule Imaging* at CFEL for giving me the opportunity of writing this bachelor thesis. I would like to thank Dr. Terence Mullins and Thomas Kierspel for their time, ideas and answers to problems with pulse duration measurements and strange stages. I am grateful for the fast integration in the group and the opportunity to participate in seminars, colloquiums and Femto12. It was a great experience and supported my choice of studying physics and the choice of writing my thesis in this interesting group completely.

I also have to thank my former physics teachers in school who made a very good job and showed me the fascinating world of physics. Without their lectures and their fun of teaching and showing experiments, I would not have considered studying physics at all.

My sincere thanks go to my fellow students who helped me finding a fun way to stay in the physics library all day, spending the weekends writing this thesis rather than going out, discussing the most weird things and having the feeling the more we learn the less we know all the time.

Last but not least I would like to thank my family and non-physicists friends who always supported me in doing what I do and tried to understand what I do, even when they had no idea, what I actually was talking about.